

Article

# Geological Controls on Mineralogy and Geochemistry of the Permian and Jurassic Coals in the Shanbei Coalfield, Shaanxi Province, North China

Yunfei Shangguan <sup>1</sup>, Xinguo Zhuang <sup>1,\*</sup>, Jing Li <sup>1</sup>, Baoqing Li <sup>1</sup>, Xavier Querol <sup>1,2</sup>, Bo Liu <sup>1</sup>, Natalia Moreno <sup>2</sup> , Wei Yuan <sup>3</sup>, Guanghua Yang <sup>4</sup> and Lei Pan <sup>4</sup>

<sup>1</sup> Key Laboratory of Tectonics and Petroleum Resources, China University of Geosciences (Wuhan), Ministry of Education, Wuhan 430074, China; SGyunfei@cug.edu.cn (Y.S.); lijing02003140@163.com (J.L.); bqli1986@126.com (B.L.); xavier.querol@idaea.csic.es (X.Q.); liubo1989@yahoo.com (B.L.)

<sup>2</sup> Institute of Environmental Assessment and Water Research, IDÆA-CSIC C/Jordi Girona, 18–26, 08034 Barcelona, Spain; natalia.moreno@idaea.csic.es

<sup>3</sup> Inner Mongolia Geology Engineering Co., Ltd., Xinhudong Street 87, Hohhot 010010, China; yuanweicumt@126.com

<sup>4</sup> Xi'an Institute of Geology and Mineral Exploration, Western Duling Road 56, Xi'an 710100, China; Fushiaihua1999@sina.com (G.Y.); plpy1985@126.com (L.P.)

\* Correspondence: xgzhuang@cug.edu.cn

Received: 3 December 2019; Accepted: 4 February 2020; Published: 6 February 2020



**Abstract:** Coal as the source of critical elements has attracted much attention and the enrichment mechanisms are of significant importance. This paper has an opportunity to investigate the mineralogical and geochemical characteristics of the Permian and Jurassic bituminous coals and associated non-coals from two underground coal mines in the Shanbei Coalfield (Northeast Ordos basin), Shaanxi Province, North China, based on the analysis of X-ray diffraction (XRD), inductively coupled plasma atomic-emission spectrometry (ICP-AES/MS), and scanning electron microscopy-energy-dispersive X-ray spectroscopy (SEM-EDS). The Jurassic and Permian coals have similar chemical features excluding ash yield, which is significantly higher in the Permian coals. Major mineral matters in the Jurassic coals are quartz, kaolinite, and calcite. By contrast, mineral assemblages of the Permian coals are dominated by kaolinite; and apatite occurring in the middle section's partings. The Jurassic coals are only enriched in B, whereas the Permian coals are enriched in some trace elements (e.g., Nb, Ta, Th, and REY). Boron has a mixed inorganic and organic association which may be absorbed by organic matter from fluid (or groundwater) or inherited from coal-forming plants. Additionally, climatic variation also plays an important role. As for the Permian coals, kaolinite and apatite as the major carriers of elevated elements; the former were derived from the sedimentary source region (the Yinshan Oldland and the Benxi formation) and later precipitated from Ca-, and P-rich solutions. We deduced that those elevated elements may be controlled by the source rock and diagenetic fluid input. The findings of this work offered new data to figure out the mechanism of trace element enrichment of coal in the Ordos basin.

**Keywords:** Shanbei Coalfield; Permian and Jurassic bituminous coal; geochemistry; mineralogy; Yinshan Oldland

## 1. Introduction

Coal and fly ash with high concentrations of critical elements (e.g., Ge, U, Li, Ga, rare earth elements and yttrium (REYs), Nb (Ta)-Zr (Hf)-REY) have attracted much attention in recent studies because of their potential as raw materials to extract these metals [1–8]. Germanium-rich coal has

been discovered and used industrially in Wulantuga, Yimin, Lincang and the Russian Far East [1,9–14]. The occurrence of uranium in coal, another metal industrially extracted from coal, was also studied by many researchers in the Yili basin, Guiding, Mopingpo [15–17]. In addition, coal from the Ordos Basin, which is the second largest sedimentary basin in China, is enriched in a number of critical elements in different coalfields, for instance, the Permo-Carboniferous coals in the Junger Coalfield, especially No. 6 coal seam, have been reported to be enriched in some critical elements in different coal mines [18–22].

The geological factors affecting enrichment of valuable metals in coals have been discussed by many researchers [5,23–27]. Dai et al. (2012) proposed five genetic types of trace elements enrichment in Chinese coals [5]. However, in some cases, the enrichment of trace elements is probably a consequence of multiple geological factors [17,19,27,28]. For example, the enrichment of some critical elements in the Junger coalfield was ascribed to a combination of the input of terrigenous detrital materials (mostly bauxite and moyite) and the leaching of groundwater [18–20]. Abundant information has been obtained in recent years on the geological factors causing elevated elements concentration in the Ordos Basin [18–20,22,29–34]. Compared with the Permo-Carboniferous coals, a few studies have been carried out on the Jurassic coals due to low ash yield and absence of geochemical anomalies [22,30,31,33–35].

The Shanbei Coalfield is located in the northeast of the Ordos Basin and is adjacent to the south part of the Junger Coalfield, where some coals rich in critical elements were found in the Heidaigou, Haerwusu, and Guanbanwusu coal mines. Thus, the Shanbei coals, especially the Permo-Carboniferous coals, would be expected to be enriched in some critical elements. Based on mineralogical and geochemical analyses of coals and associated non-coals from two different coal mines, this paper discusses the heterogeneity of geochemical and mineralogical compositions of coals formed in different periods, and investigates the geological factors controlling the enrichment of some trace elements.

## 2. Geological Setting

The Shanbei Coalfield, located in the northeast of the Ordos Basin, consists of the Shanbei Permo-Carboniferous, Shanbei Triassic and Shanbei Jurassic Coalfields, the first of which belongs to the Jinxi Fold Belt and the latter two to the Yishan Slope (Figure 1). The main coal-bearing strata in this region consist of the Late Carboniferous Taiyuan ( $C_{2t}$ ), the Early Permian Shanxi ( $P_{1sh}$ ), the Late Triassic Wayaobao ( $T_{3w}$ ), and the Middle Jurassic Yan'an Formations ( $J_{2y}$ ). The Cuijiagou underground coal mine is located in the northeastern part of the Shanbei Jurassic Coalfield, and the Puran coal mine is located in the north of the Shanbei Permo-Carboniferous Coalfield (Figure 1).

Based on the occurrence of different types of fossils, the Taiyuan Formation is subdivided into three members (Figure 2A), all of which were deposited in lagoon and tidal flat-barrier environments [35]. Member 1 overlies conformably the Benxi Formation limestone and is composed of bauxite, sandstone and coal seams (No. 10 and 11 Coal); member 2 is the main limestone-bearing section, which consists of limestone, sandstone, mudstone and, 3 coal seams (No. 9, 8, and 7 Coals); and member 3 contains limestone and one coal seam (No. 6 Coal) which has been extensively studied [18,19].

The Shanxi Formation, subdivided into 2 members, consists mainly of sandstone and several coal seams (Nos. 1 to 5, Figure 2A). The No. 3, No. 4, and No. 5 coal seams within member 1 are the main workable coals, while other coal seams are mostly unminable. The Shanxi Formation was mainly formed in a fluvial-delta environment.

The Jurassic Yan'an Formation is subdivided into 5 members according to coal-bearing characteristics and lithological compositions (Figure 2B), all of which are composed of sandstone, mudstone, and five coal seams (Nos. 5 to 1 coals from bottom to top). The No. 1 and No. 3 coals were formed in the delta plain while No. 2 in the shallow lake environment [36].

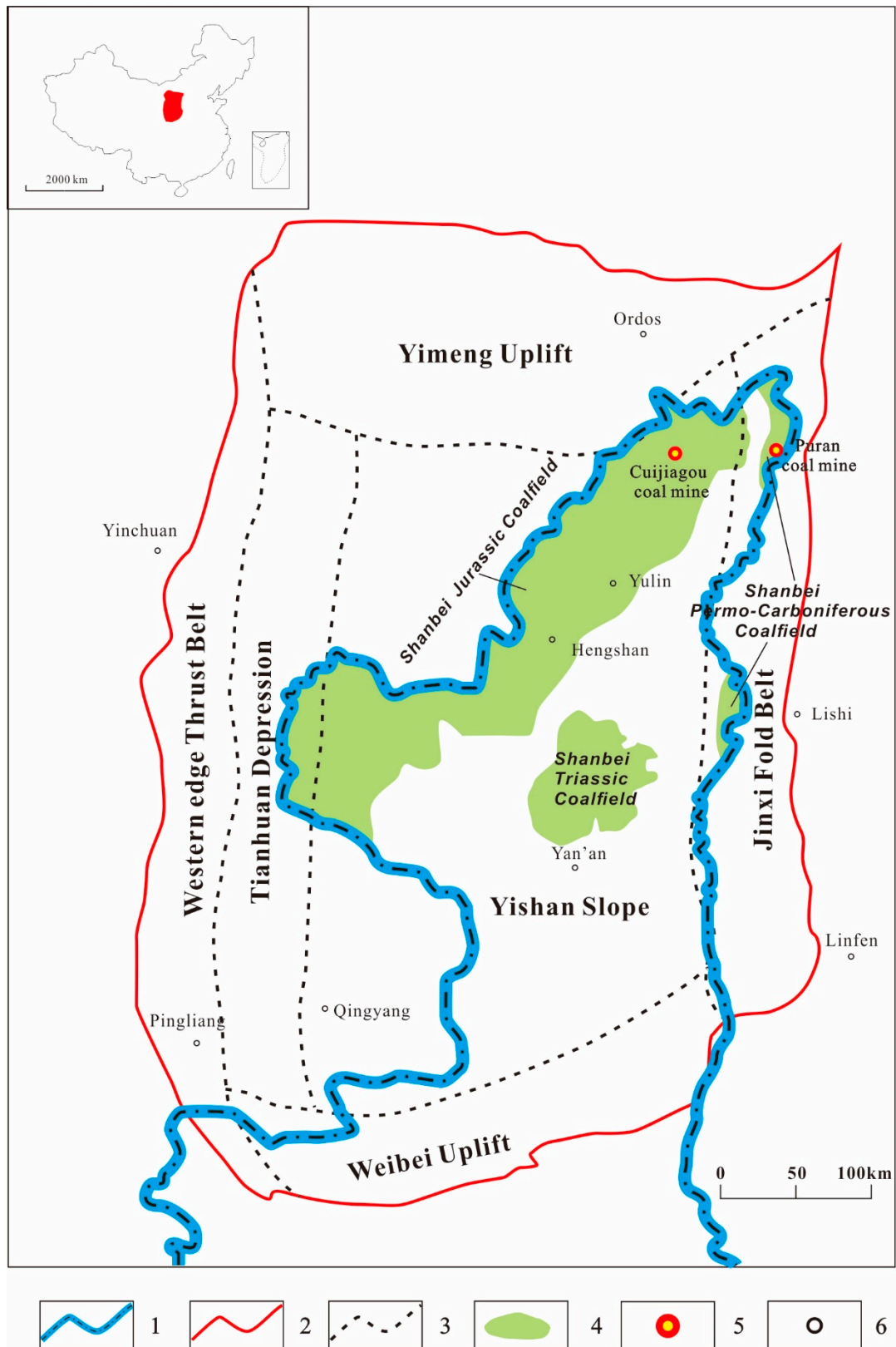


**Figure 1.** Geological map of Ordos Basin showing the location of the Shanbei Coalfield (Modified from Wang et al., [35]). 1. province boundary; 2. Ordos basin boundary; 3. tectonic unit boundary; 4. Shanbei Coalfield; 5. study coal mine; 6. main city in Ordos basin.

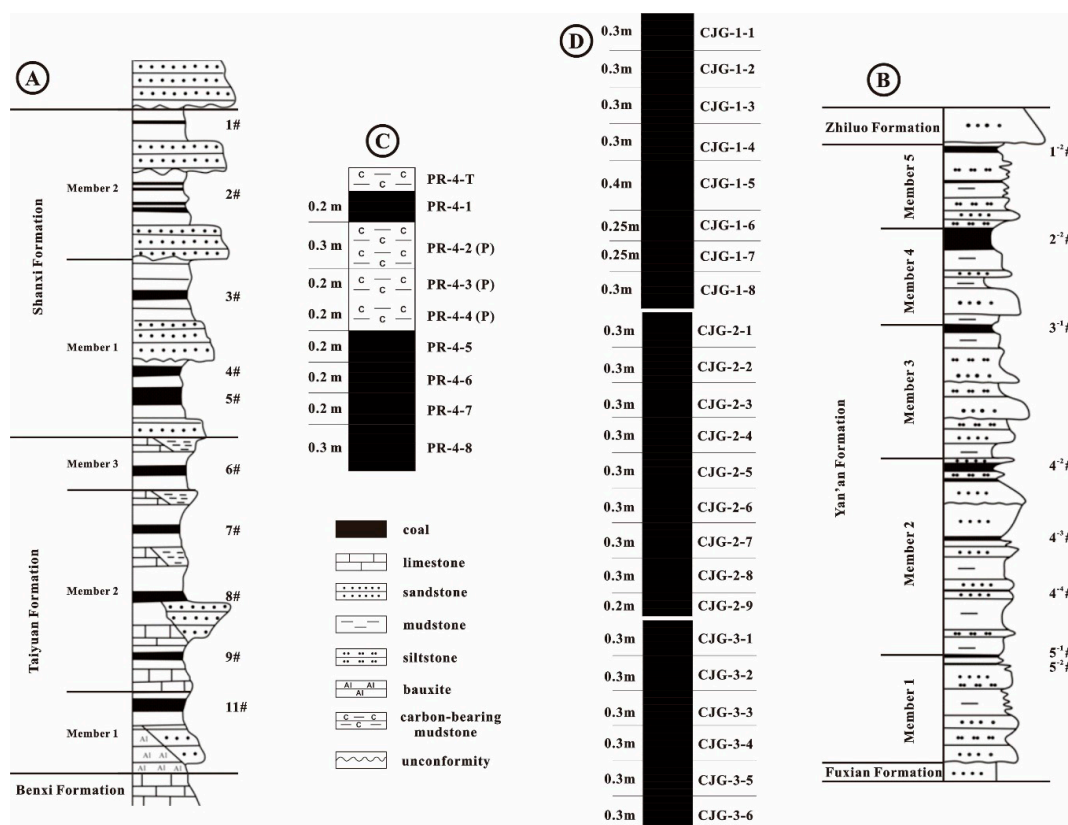


**Figure 2.** Sedimentary sequence of the Taiyuan and Shanxi Formations (A) and Yanan Formation (B) in the Ordos Basin [35] and sampling location from the Puran (C) and Cuijiagou (D) underground coal mines [35].

### 3. Samples and Methods

A total of 32 channel samples were collected from the Cuijiagou (Shanbei Jurassic Coalfield) and the Puran (Shanbei Permo-Carboniferous Coalfield) underground coal mines, including 23 coal samples from the Cuijiagou, 5 coal samples, 3 parting samples (with a suffix P), and one roof sample (with a suffix T) from the Puran mine. According to the natural stratification of the Cuijiagou coals, 8 (identified as CJG-1-1 to CJG-1-8), 9 (identified as CJG-2-1 to CJG-2-9), and 6 (identified as CJG-3-1 to CJG-3-6) coal samples were respectively collected from Nos. 1, 2, and 3 coal seams from the top to bottom. In the Puran coal mine, one roof sample (PR-4-T) and 8 coal (PR-4-1, PR-4-5 to PR-4-8) and parting samples (PR-4-2 to PR-4-4) were collected from the No. 4 coal from top to bottom. The thickness of individual samples is shown in Figure 2C,D).

The samples were crushed and ground to pass through an 80-mesh sieve for proximate analysis. Thereafter the remaining splitting samples were further milled to pass through a 200-mesh sieve for geochemical and mineralogical analyses. Proximate analysis was carried out according to ASTM (American Society for Testing and Materials) Standards D3173/D3173M-17a (2017), D3174-12 (2018), and D3175-18 (2018) [37–39]. Powder X-ray diffraction (XRD), using a Bruker D8 Advance A25 powder diffractometer (Bruker AXS GmbH, Karlsruhe, Germany) with monochromatic CuK $\alpha$  radiation operated at 40 kV and 40 mA, scanning from 4° to 60° 2 theta with a step size of 0.05° and a counting time of 3 s/step, was used to determine minerals compositions of the collected samples. Meanwhile, semi-quantitative XRD estimation of the mineral contents was obtained by using the reference internal standard method [40]. In order to identify the morphology and composition of individual minerals, some perpendicular to coal layer polished fragments obtain from relatively higher mineral content samples were studied by a field emission-scanning electron microscope (FE-SEM, FEI Quanta™ 450

FEG, Thermo Fisher, Hillsboro, OR, USA) with an energy-dispersive X-ray spectrometer (EDAX; Genesis Apex 4, Mahwah, NJ, USA).

With respect to the major and trace elements concentrations, a two-step digestion method proposed by Querol et al. (1997) was used to retain volatile elements in the solution [41]. Subsequently, the contents of major and selected trace elements were detected by inductively coupled plasma atomic-emission spectrometry (ICP-AES, Iris Advantage Radial ER/S device from Thermo Jarrell-Ash, Waltham, MA, USA), and the contents of most trace elements by inductively coupled plasma mass spectrometry (ICP-MS, X-SERIES II Thermo Fisher Scientific, Bremen, Germany). In order to guarantee the accuracy of the digestion and the analytical methods, digestion of blank samples and international reference materials (SARM-19) was also carried out following the same procedure.

## 4. Results

### 4.1. Coal Quality and Rank

The Jurassic coals (Nos. 1, 2, and 3) are characterized by low moisture contents (7.2%, 5.8%, and 6.0%, respectively), low high-temperature ash (HTA, under 750 °C) yields (3.8%, 7.4%, and 3.1%, respectively), and high volatile matter yields (33.8%, 40.7%, and 36.9%, respectively) (Table 1), indicating that the Jurassic coals are high volatile bituminous coals (ASTM, 2011). All coal seams have similar total S contents ranging from 0.3% to 0.8%, indicating low-sulfur coals according to Chou (2012) [42].

**Table 1.** Proximate analysis (%) and S content (%) of the coal samples in the studied mines. M, moisture; A, ash yield; V, volatile yield; St, total sulfur; ad, air dry basis; d, dry basis; daf., dry and ash-free basis.

Sample	M <sub>ad</sub> %	A <sub>d</sub> %	V <sub>daf</sub> %	St <sub>d</sub> %
CJG-1-1	7.40	5.10	35.00	0.81
CJG-1-2	7.20	4.00	32.30	0.28
CJG-1-3	6.80	3.30	30.50	0.29
CJG-1-4	6.80	4.80	32.20	0.27
CJG-1-5	7.10	3.70	34.60	0.34
CJG-1-6	6.70	3.30	28.40	0.23
CJG-1-7	8.50	2.00	38.60	0.43
CJG-1-8	7.20	4.00	39.10	0.40
<b>Average</b>	<b>7.21</b>	<b>3.78</b>	<b>33.84</b>	<b>0.38</b>
CJG-2-1	5.40	6.00	38.30	0.38
CJG-2-2	5.30	21.90	47.00	0.27
CJG-2-3	5.50	7.10	38.70	0.29
CJG-2-4	6.20	17.00	43.50	0.28
CJG-2-5	5.10	5.00	40.60	0.51
CJG-2-6	7.00	2.30	38.90	0.28
CJG-2-7	6.10	2.70	41.30	0.27
CJG-2-8	6.00	2.30	40.10	0.35
CJG-2-9	5.60	2.40	37.90	0.34
<b>Average</b>	<b>5.80</b>	<b>7.41</b>	<b>40.70</b>	<b>0.33</b>
CJG-3-1	5.60	4.80	37.20	0.28
CJG-3-2	5.50	4.10	32.70	0.23
CJG-3-3	6.00	3.00	36.70	0.25
CJG-3-4	6.30	2.00	36.00	0.22
CJG-3-5	6.30	1.80	37.30	0.29
CJG-3-6	6.20	2.70	41.60	0.31
<b>Average</b>	<b>5.98</b>	<b>3.07</b>	<b>36.92</b>	<b>0.26</b>
PR-4-T	1.10	79.50	76.70	0.05
PR-4-1	1.80	45.00	40.30	0.30
PR-4-2(P)	1.40	76.90	69.90	0.05
PR-4-3(p)	1.70	69.80	55.90	0.07
PR-4-4	1.80	61.60	48.90	0.20
PR-4-5	2.10	30.70	38.70	0.33
PR-4-6	2.40	22.10	41.70	0.35
PR-4-7	2.70	18.80	41.30	0.34
PR-4-8	2.90	15.30	41.90	0.44
<b>Average (coals)</b>	<b>2.38</b>	<b>26.38</b>	<b>40.78</b>	<b>0.35</b>

By contrast, the Permian No. 4 coal in the Puran coal mine has lower moisture content (2.3% ad, on average) and higher ash yield (24.4%), which is also higher than the coals of late Carboniferous Taiyuan Formation in the Jungar Coalfield [18–20,22]. In addition, the ash yields show an increasing trend from PR-4-8 (15.3%) to PR-4-1 (45.0%). The Permian coals have high volatile matter yields ranging from 38.7% to 41.9% (daf.), indicating that the coal rank belongs to high volatile bituminous coal (ASTM, 2011). The total S contents of the Permian coals range 0.3% to 0.4% (Table 1), also indicating low-sulfur coal [42].

## 4.2. Mineralogy

### 4.2.1. Mineralogical Compositions and Vertical Distribution

In this study, we using major (>10%, dry basis-db), minor (1–10%, db), and trace (<1%, db) amount of mineral to group all minerals. In the Permian coals, minerals consist mainly of kaolinite (average of 23.6%, db) and traces of calcite, and apatite only detected in the PR-4-5 and PR-4-6 (Table 2). Trace amounts of zircon and boehmite are observed in some samples using scanning electron microscopy-energy-dispersive X-ray spectroscopy (SEM-EDS). The major minerals in the roof sample (PR-4-T) are kaolinite (68.3%, db.), followed by tobelite, and minor amount of dolomite. The parting samples mainly consist of kaolinite (75.9%, 68.7%, 59.8%, db.), and PR-4-4 (P) contains trace amount of apatite. Zircon, galena, dolomite, and anatase in the partings were also occasionally identified by SEM-EDS analysis. In addition, the vertical variation of kaolinite content is consistent with ash yield, increasing from bottom to the top. Calcite was detected in the top and bottom of the coal seam but is absent in the middle parting samples.

The Jurassic coals contain variable mineral assemblages among different coal seams. The No. 1 coal consists of minor calcite (2.3% db.) and trace amount of quartz (0.9% db), and to a lesser extent, kaolinite, pyrite and gypsum only present in a few samples. The mineral in the No. 2 coal mainly consists of calcite, quartz, and kaolinite, with the exceptions of samples CJG-2-2 and CJG-2-4, the former of which is primarily dominated by calcite (17.6%, db) and to a less extent, ankerite (3.1% db), and the latter of which is dominated by siderite (4.4%, db). Traces of dolomite, pyrite, and gypsum were also detected in some samples. The No. 3 coal mainly consists of quartz (2.4%, db), with trace amounts of kaolinite and calcite, pyrite, and gypsum only present in a few samples (Table 2). Vertically, calcite is concentrated in No. 1 and top of No. 2 (top) coals. The amount of quartz is markedly higher near the floor and roof rocks of the No. 1 and 3 coals, possibly indicating some input of terrigenous detrital materials as the peat was being established or being progressively overwhelmed by other depositional environments as reported by Ward and Christie [43]. The content of kaolinite decreases from the bottom to the top in the No. 1 and 2 coal seams, but shows no obvious variation in the No. 3 coal seam.

### 4.2.2. The Modes of Occurrence of Minerals

#### Silicate Minerals

Kaolinite is the major constituent in the Jurassic and Permian coals and occurs in the following three types: (I) as lumps and thin-layered forms in collodetrinite (Figures 3A and 4A,B), with the size ranging from 1  $\mu\text{m}$  to 200  $\mu\text{m}$ , indicating a terrigenous detrital origin; (II) as fracture/cleat infillings (Figure 5A–C), indicating an epigenetic precipitation from the migrating diagenetic/epigenetic fluids. (III) as cell infillings, in a few cases, along with apatite (Figure 3AB–D, Figure 4C,D and Figure 6A,B), indicating an authigenic origin during syngenetic to early diagenetic stages; and unlike in the coal samples, kaolinite occurs primarily as discrete particles and thin layers (Figure 7A), sometimes as vermicular form in the non-coal rock samples (Figure 7B).

Quartz associated with organic matter as euhedral crystals (Figure 3E), analogous to that of volcanic origin with relatively short transport from source region. It is also found as rounded fine

grains (<5  $\mu\text{m}$ , Figures 3A and 5D) typical of a detrital origin with relatively long transport from source region.

Chamosite has been identified by SEM-EDS analysis and is present as cell fillings, sometimes co-existing with kaolinite (Figure 5A). A similar mode of occurrence has also been identified in some coals [44,45]. The coexistence of kaolinite and chamosite possibly indicates that chamosite was derived from the interaction of pre-existing kaolinite and Fe-Mg-rich fluids during early diagenesis [46].

Zircon primarily occurs as euhedral crystals within the kaolinite matrix (Figure 8A) and organic matter (Figure 9A). The SEM-EDS data show that zircon grains contain Y, Nb, Hf, P and Sc (Figures 8A and 9A).

Tobelite, although only detected in the roof sample PR-4-T by XRD, is a typical mineral in tonsteins of Permo-Carboniferous coal accumulation area of Northern China [47]. Based on the previously published literature, tobelite is almost exclusively observed in high-rank coals and formed by interaction of already present K-illite and/or kaolinite with nitrogen which released by decomposition of organic matter during rank advance or hydrothermal alteration [48–53]. In present study, illite has not been detected by XRD or SEM-EDS, we deduced that tobelite may be formed from the interaction of kaolinite and nitrogen which is similar to the Permian coals in Tongzi Coalfield [51].

#### Carbonate Minerals

The carbonate minerals detected by XRD include calcite, siderite, ankerite, and dolomite. Siderite occurs as cavities infillings of kaolinite (Figure 3F). Calcite occurs as fracture infillings (Figure 5B). Dolomite has euhedral crystals morphology and precipitated along fractures in the organic matter matrix (Figure 4E), indicating epigenetic precipitation from Ca-Fe-rich solutions.

#### Sulfide Minerals

Pyrite is only detected in the Jurassic coals and occurs as framboidal euhedral crystals within organic matter (Figure 3D,F). Here, the framboidal pyrite with a relatively uniform distribution closely to one another is different with the bacteriogenic framboidal pyrite which occurs as separated globules described by Kostava et al. [54], indicating authigenic origin during syn-depositional or early diagenetic stage. Galena, containing Cu and Hg, occurs as crystals included within the kaolinite matrix (Figure 7B–D), indicating an authigenic origin.

#### Oxide and Hydroxide Minerals

Anatase grains occur in the kaolinite matrix in the parting samples (Figure 7E) and contain traces of La, Ce, and V (Figure 8B).

Boehmite is detected by SEM-EDS in the Permian coals and mainly occurs as finely disseminated grains within the kaolinite matrix (Figure 9B), possibly indicating a detrital origin. It has also been found in other Permian coals in the Jungar Coalfield and Weibei Coalfield [3,18–21,52].

#### Sulfate Minerals

Gypsum occurs as lamellar aggregate infilling the fracture alone or together with kaolinite (Figure 5C,E,F). Sometimes, gypsum has been considered as the produce of the storage of coal [55] or derived from marine water before compaction [56], however, the two genesis types were excluded based on the following evidence: on the one hand, the morphology of marine derived gypsum, which occurs in platy crystals as fillings in plant cells and vugs, is different from this study, and on the other hand, the absence of calcite and pyrite in this sample. Thus, gypsum in this study has an authigenic origin involving precipitated from the Ca-rich solutions.

## Phosphate Mineral

Phosphates are represented by apatite in the Permian coals and occur as cell-fillings (Figure 6C,D and Figure 7F) which represents syngenetic precipitation in the peat bed, and individual grains with angular shape (Figure 6E). Some apatite occurs in the matrix of kaolinite (Figures 4C and 6F) or organic matter matrix (Figures 4F and 9C). In addition, apatite in the partings contains Zr, Y, and Nb (Figure 8C) whereas in coal sample contain Zr (Figure 9C).

**Table 2.** Mineral contents in coals and non-coals as determined by X-ray diffraction (XRD) from the two coal mines (on whole-coal basis; unit in %, db.). The Numbers in this Table represent results of XRD; \* represent mineral detected by scanning electron microscopy-energy-dispersive X-ray spectroscopy (SEM-EDS).

Sample	Kaolinite	Calcite	Dolomite	Tobelite	Apatite	Galena	Anatase	Zircon	Boehmite
PR-4-T	68.3		1.7	8.6					
PR-4-1	43	1.3							
PR-4-2 (P)	75.9								
PR-4-3 (P)	68.7								
PR-4-4 (P)	59.8				0.7	*	*	*	
PR-4-5	27.3				2.8				
PR-4-6	20.6	0.3	*		0.7			*	*
PR-4-7	17.9	0.5							
PR-4-8	9.4	5.5							
Sample	Quartz	Kaolinite	Calcite	Pyrite	Gypsum	Siderite	Chamosite		
CJG-1-1	1.6	0.4	2.3	0.3	0.1	*			
CJG-1-2	1.3	0.6	1.8						
CJG-1-3	0.5	0.4	2.2						
CJG-1-4	1.3	0.6	2.6						
CJG-1-5	0.4	0.2	2.9						
CJG-1-6	0.5	0.5	2						
CJG-1-7	0.9	0.8							
CJG-1-8	2.2	1.6							
CJG-3-1	4.1	0.4		0.1					
CJG-3-2	3.2	0.6		0.1	0.1				
CJG-3-3	2	0.6	0.2						
CJG-3-4	1.5	0.3					*		
CJG-3-5	1.2	0.5							
CJG-3-6	2.5	0.1							
Sample	Quartz	Kaolinite	Calcite	Dolomite	Pyrite	Siderite	Ankerite	Gypsum	
CJG-2-1	0.3	0.2	4.6				0.6		
CJG-2-2			17.6				3.1		
CJG-2-3	0.1	0.4	5.6			0.1	0.3		
CJG-2-4	3.4	0.5	7.2	0.2		4.4		0.2	
CJG-2-5	3.5	0.7	0.2		0.1			0.2	
CJG-2-6	1.1	0.4	0.6		0.1				
CJG-2-7	2.3	0.1			0.1				
CJG-2-8		2.1							
CJG-2-9	1.4	0.9							

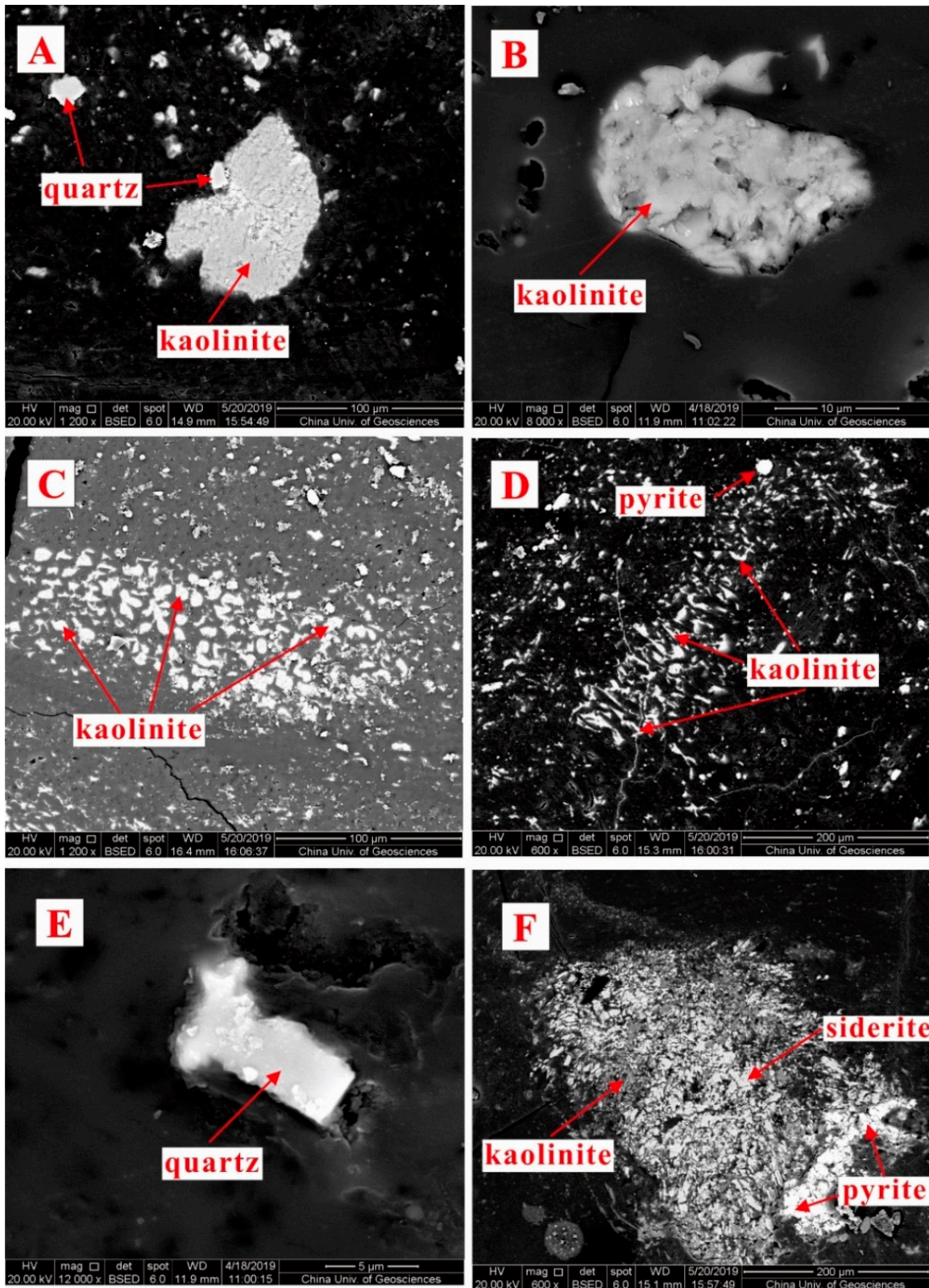


**Figure 3.** SEM back-scattered images of kaolinite, quartz, pyrite and siderite in the sample of CJK-1-1. (A) dispersed kaolinite and quartz particles; (B,C) syngenetic cell-filling kaolinite; (D) syngenetic cell-filling kaolinite and detrital pyrite grain; (E) authigenic quartz; (F) mineral assemblage including siderite, kaolinite, and framboidal pyrite.

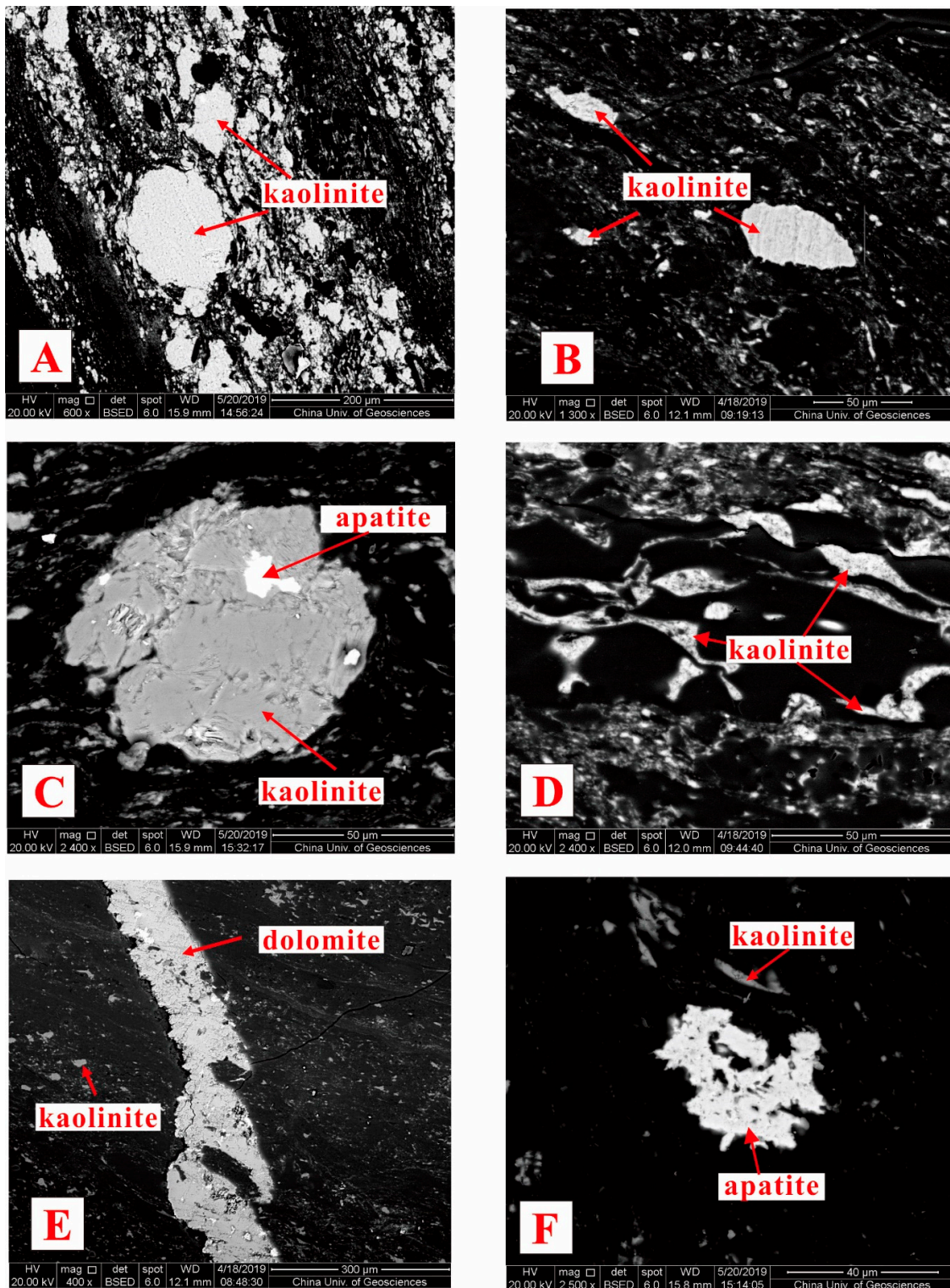


**Figure 4.** SEM back-scattered images of kaolinite, apatite and dolomite in PR-4-6. (A,B) dispersed kaolinite particles or kaolinite lenses; (C) apatite filling cavities of kaolinite; (D) cell-filling kaolinite; (E) fracture-filling dolomite; (F) apatite fillings pore/cavity of organic matter.

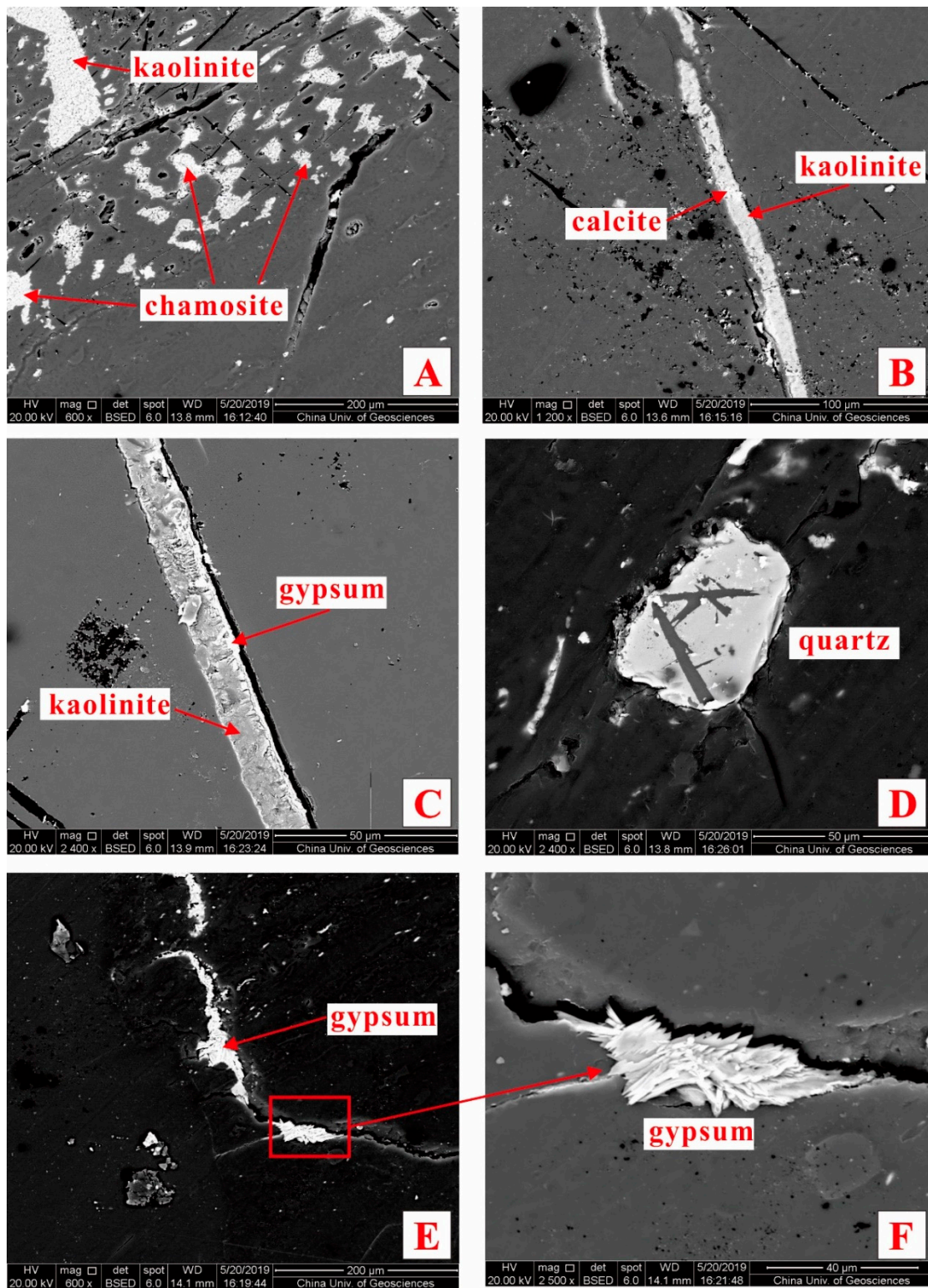


**Figure 5.** SEM back-scattered images of kaolinite, chamosite, calcite, gypsum and quartz (sample CJG 3-4). (A) syngenetic cell-filling chamosite and cleat/fracture-filling kaolinite; (B,C,E,F) cleat/fracture-filling kaolinite, gypsum and calcite; (D) Sub-round quartz grain associated with organic matter.

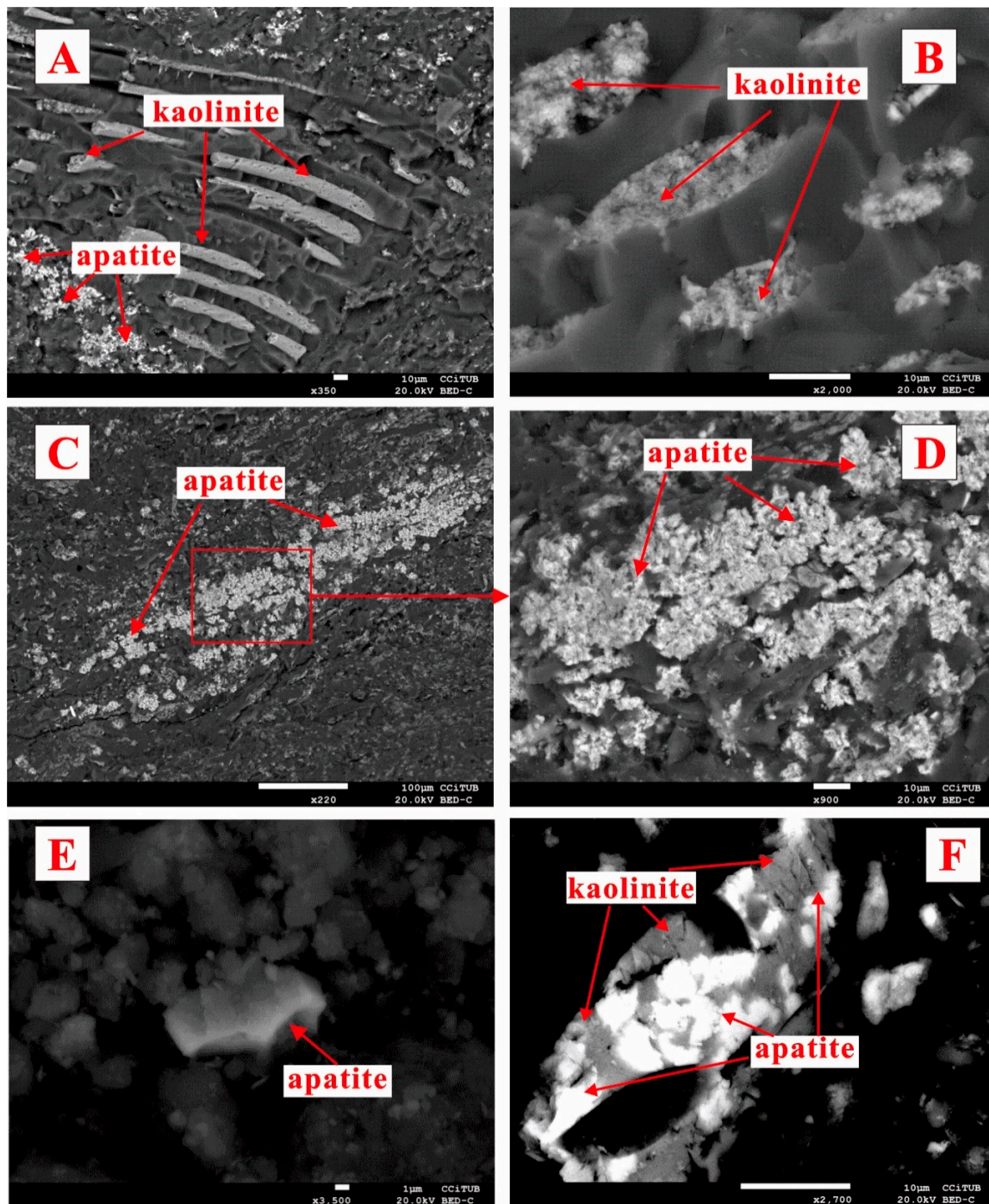


**Figure 6.** SEM back-scattered images of kaolinite and apatite (sample PR 4-5-P). (A,B) cell-filling kaolinite; (C,D) syngenetic cell or pore space infillings apatite; (E) dispersed apatite particles within organic matter; (F) the growth of kaolinite and apatite.

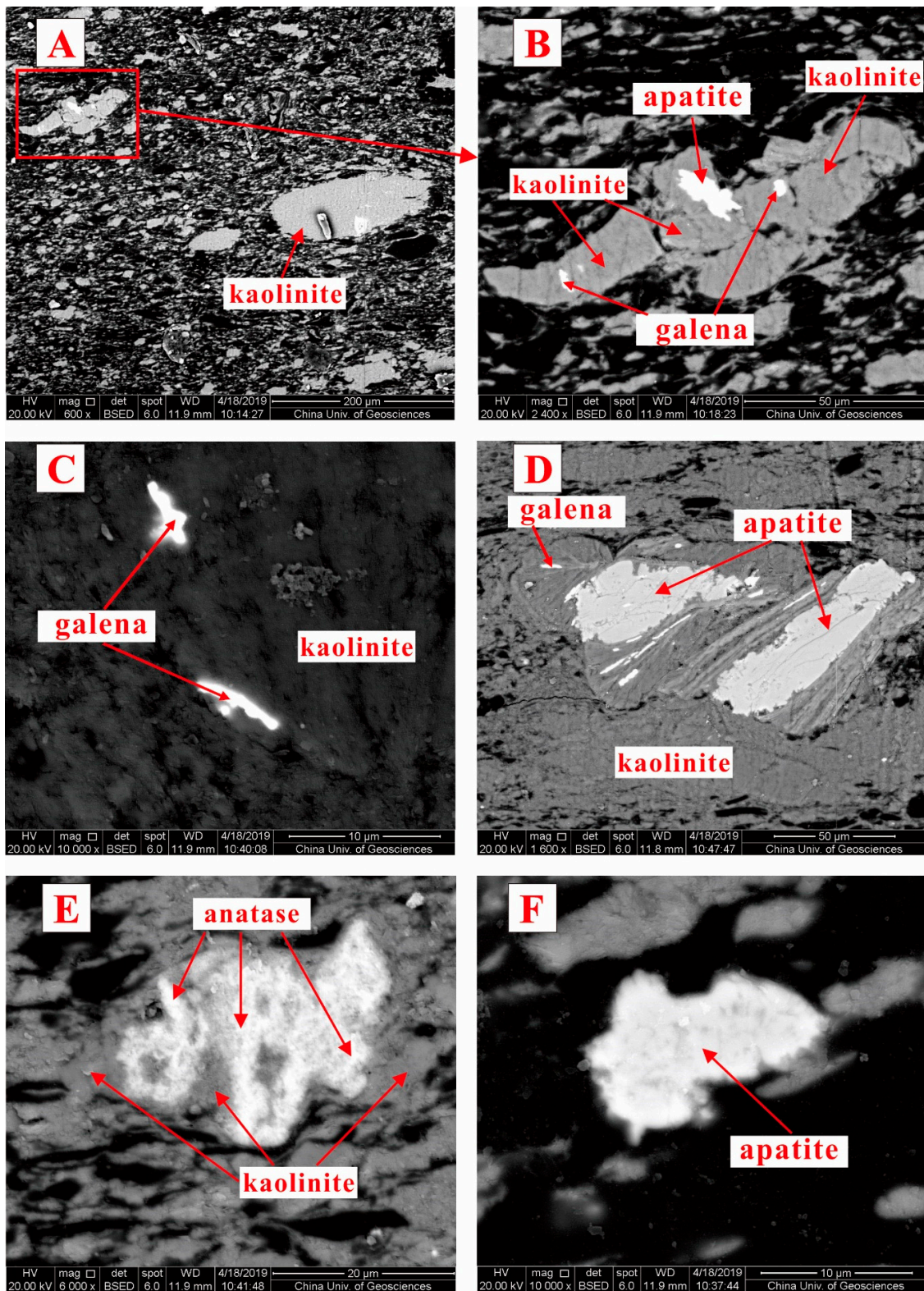


**Figure 7.** SEM back-scattered images of kaolinite, apatite, galena and anatase in the parting sample of PR-4-4 (P). (A) dispersed kaolinite particles; (B) vermicular kaolinite; (C,D) apatite, galena fillings cavity of kaolinite; (E) kaolinite matrix, anatase filling the cavities of kaolinite matrix; (F) cell-filling apatite.

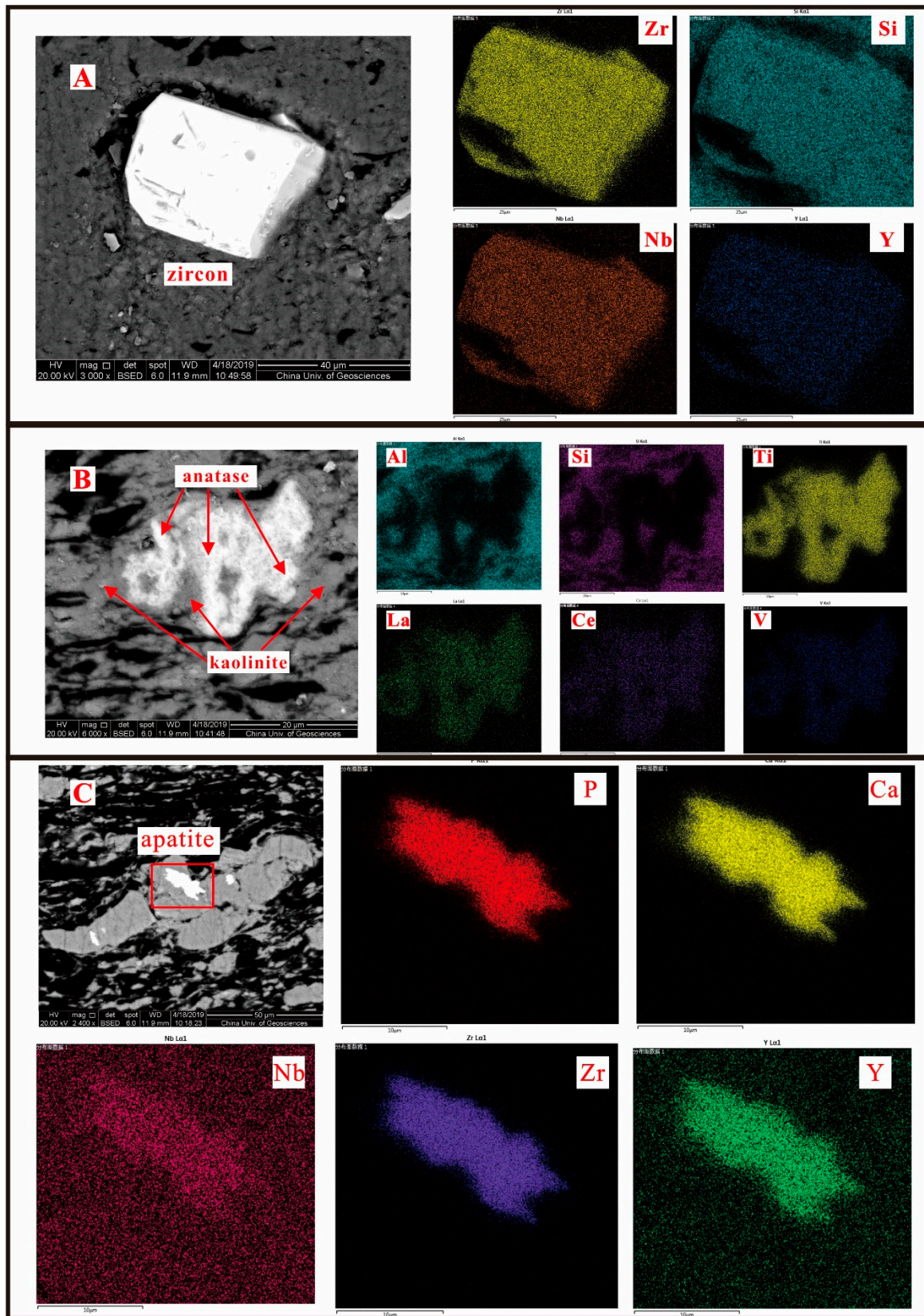
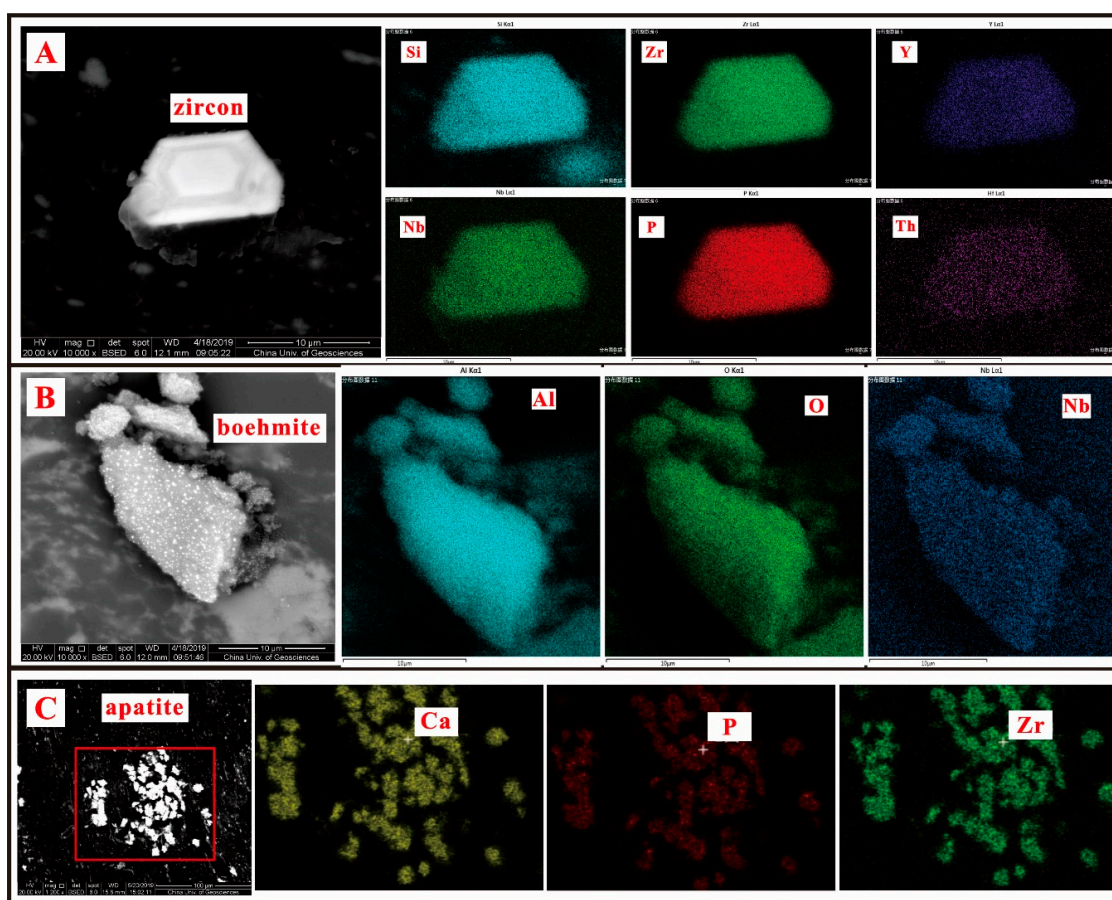


Figure 8. SEM-EDS mappings of zircon (A), anatase (B), and apatite(C) in the parting sample PR-4-4.



**Figure 9.** SEM-EDS mappings of zircon (A), boehmite (B) and apatite (C) in the coal sample of PR-4-6.

### 4.3. Geochemistry

#### 4.3.1. Major and Trace Element Concentration

The major elements in No. 4 coal seam of the Puran coal mine are dominated by  $\text{Al}_2\text{O}_3$  (13%) and  $\text{SiO}_2$  (11%), followed by CaO and  $\text{Fe}_2\text{O}_3$ , with trace amounts of  $\text{K}_2\text{O}$ , MgO and  $\text{Na}_2\text{O}$  (Table 3), as would be expected from the mineral composition that is dominated by kaolinite (Table 2). By contrast, the Cuijiagou coals (No. 1, No. 2, and No. 3 coals) have lower contents of most major elements due to lower ash yields. More specifically, the major elements of No. 1 coal seam are  $\text{SiO}_2$  (1.3%) and  $\text{Al}_2\text{O}_3$  (1.2%), followed by CaO and  $\text{Fe}_2\text{O}_3$ , with trace amounts of  $\text{K}_2\text{O}$ , MgO and  $\text{Na}_2\text{O}$ . The No.2 coal seam has higher contents of CaO (3.1%) and  $\text{Fe}_2\text{O}_3$  (2.1%), which may have been caused by higher amounts of carbonate minerals (such as siderite, calcite, dolomite and ankerite) and pyrite. The No. 3 coal seam is mainly dominated by  $\text{SiO}_2$  (2.5%).

The  $\text{SiO}_2/\text{Al}_2\text{O}_3$  ratios of No. 4 coal seam (Table 3, 1.5) in the Permian coals are approximately equivalent to that for the Chinese coals (1.4) [5] but slightly higher than the theoretical ratio for kaolinite (1.2). The  $\text{SiO}_2/\text{Al}_2\text{O}_3$  ratio is elevated by sample PR-4-7 with  $\text{SiO}_2/\text{Al}_2\text{O}_3$  ratio of 3.7. The middle and upper portions have lower ratios of  $\text{SiO}_2/\text{Al}_2\text{O}_3$  (Table 3, 0.6–0.9) due to the presence of Al-oxyhydroxide such as boehmite (Figure 9B). The  $\text{SiO}_2/\text{Al}_2\text{O}_3$  ratio in the No. 1 (1.1), No. 2 (1.5), and No. 3 (2.9) coal seam of the Jurassic coals are close to or even higher than the theoretical ratio for kaolinite, indicating the existence of free  $\text{SiO}_2$ .

Concentration coefficient (CC) was proposed by Dai et al. [16] in the present study. Comparing with the average of Chinese coals [5], most trace elements are depleted in the Jurassic coals with  $\text{CC} < 0.5$  (Figure 10). Beryllium, B, Cr, Ta, and W in the No. 1 coal seam, Be and Sr in the No. 2 coal seam, and B, Sr Ta and W in the No. 3 coal seam are similar to the averages for Chinese coals [5]. Boron in

the No. 2 coal seam is slightly enriched. The Permian coals are enriched in Ta, slightly enriched in P, Ga, Zr, Nb, and W. The remaining trace elements are similar or less than the average for Chinese coals (Figure 11) [5]. Vertically, the elevated elements, such as Nb, Ta, Ga, Zr and REY, are mainly concentrated in coal benches close to the partings of the No. 4 coal seam.

**Table 3.** Major elements (% db) content and geochemical ratios in coal and non-coal samples from the two studied coal mines.

Sample	SiO <sub>2</sub>	Al <sub>2</sub> O <sub>3</sub>	CaO	Fe <sub>2</sub> O <sub>3</sub>	K <sub>2</sub> O	MgO	Na <sub>2</sub> O	SiO <sub>2</sub> /Al <sub>2</sub> O <sub>3</sub>	Al <sub>2</sub> O <sub>3</sub> /TiO <sub>2</sub>
CJG-1-1	1.75	1.12	1.09	1.39	0.04	0.06	0.07	1.6	29.5
CJG-1-2	1.56	1.49	0.79	0.27	0.04	0.06	0.07	1.1	64.1
CJG-1-3	0.67	1.11	0.82	0.31	0.04	0.05	0.06	0.6	97.3
CJG-1-4	1.45	1.48	1.25	0.30	0.04	0.06	0.07	1	60.2
CJG-1-5	0.46	0.73	1.50	0.38	0.04	0.05	0.07	0.7	61.4
CJG-1-6	0.75	0.96	0.99	0.18	0.05	0.05	0.07	0.8	83.8
CJG-1-7	1.28	0.83	0.23	0.25	0.04	0.04	0.06	1.6	31.2
CJG-1-8	2.78	2.10	0.28	0.28	0.04	0.06	0.08	1.4	63.2
Average	1.34	1.23	0.87	0.42	0.04	0.05	0.07	1.1	54.4
CJG-2-1	0.38	0.61	2.82	1.37	0.04	0.17	0.26	0.7	38.2
CJG-2-2	0.00	0.48	15.44	3.21	0.04	0.83	0.13	0	117.9
CJG-2-3	0.32	1.42	3.35	0.97	0.04	0.14	0.23	0.2	133
CJG-2-4	3.48	2.24	4.47	10.44	0.04	0.22	0.17	1.6	49.8
CJG-2-5	3.70	1.30	0.40	1.29	0.05	0.04	0.22	2.9	26.1
CJG-2-6	1.22	0.61	0.41	0.41	0.04	0.02	0.20	2.1	44.2
CJG-2-7	2.29	0.76	0.26	0.42	0.04	0.03	0.22	3.1	25.1
CJG-2-8	0.96	1.15	0.22	0.56	0.04	0.03	0.20	0.9	73.5
CJG-2-9	1.76	1.08	0.22	0.42	0.05	0.02	0.22	1.7	70.6
Average	1.57	1.07	3.06	2.12	0.04	0.17	0.20	1.5	48.1
CJG-3-1	4.12	1.41	0.16	0.46	0.04	0.04	0.22	3	40.6
CJG-3-2	3.31	1.20	0.21	0.62	0.04	0.07	0.22	2.9	44.4
CJG-3-3	2.18	0.79	0.25	0.68	0.04	0.06	0.20	2.9	43.8
CJG-3-4	1.60	0.59	0.15	0.48	0.04	0.04	0.19	2.8	47.8
CJG-3-5	1.35	0.60	0.13	0.54	0.04	0.03	0.18	2.3	53.9
CJG-3-6	2.44	0.69	0.14	0.33	0.04	0.02	0.16	3.7	49.6
Average	2.50	0.88	0.17	0.52	0.04	0.04	0.19	2.9	44.4
PR-4-T	34.85	51.60	0.14	0.81	0.13	0.07	0.13	0.7	46.2
PR-4-1	19.27	27.25	0.38	0.76	0.20	0.09	0.11	0.7	24.3
PR-4-2 (P)	34.02	39.45	0.13	0.67	0.14	0.07	0.12	0.9	33.3
PR-4-3 (P)	30.79	37.39	0.34	0.89	0.95	0.15	0.16	0.9	40.1
PR-4-4 (P)	26.84	39.15	0.76	0.88	0.19	0.07	0.11	0.7	38.6
PR-4-5	12.25	21.16	1.90	0.42	0.11	0.04	0.07	0.6	63.8
PR-4-6	9.22	10.41	0.62	0.37	0.04	0.04	0.06	0.9	35.1
PR-4-7	8.01	2.27	0.35	0.17	0.05	0.02	0.06	3.7	36.5
PR-4-8	4.22	2.40	1.48	0.35	0.04	0.05	0.05	1.8	45.5
Average (coal)	10.59	12.70	0.94	0.41	0.09	0.05	0.07	1.5	41.0

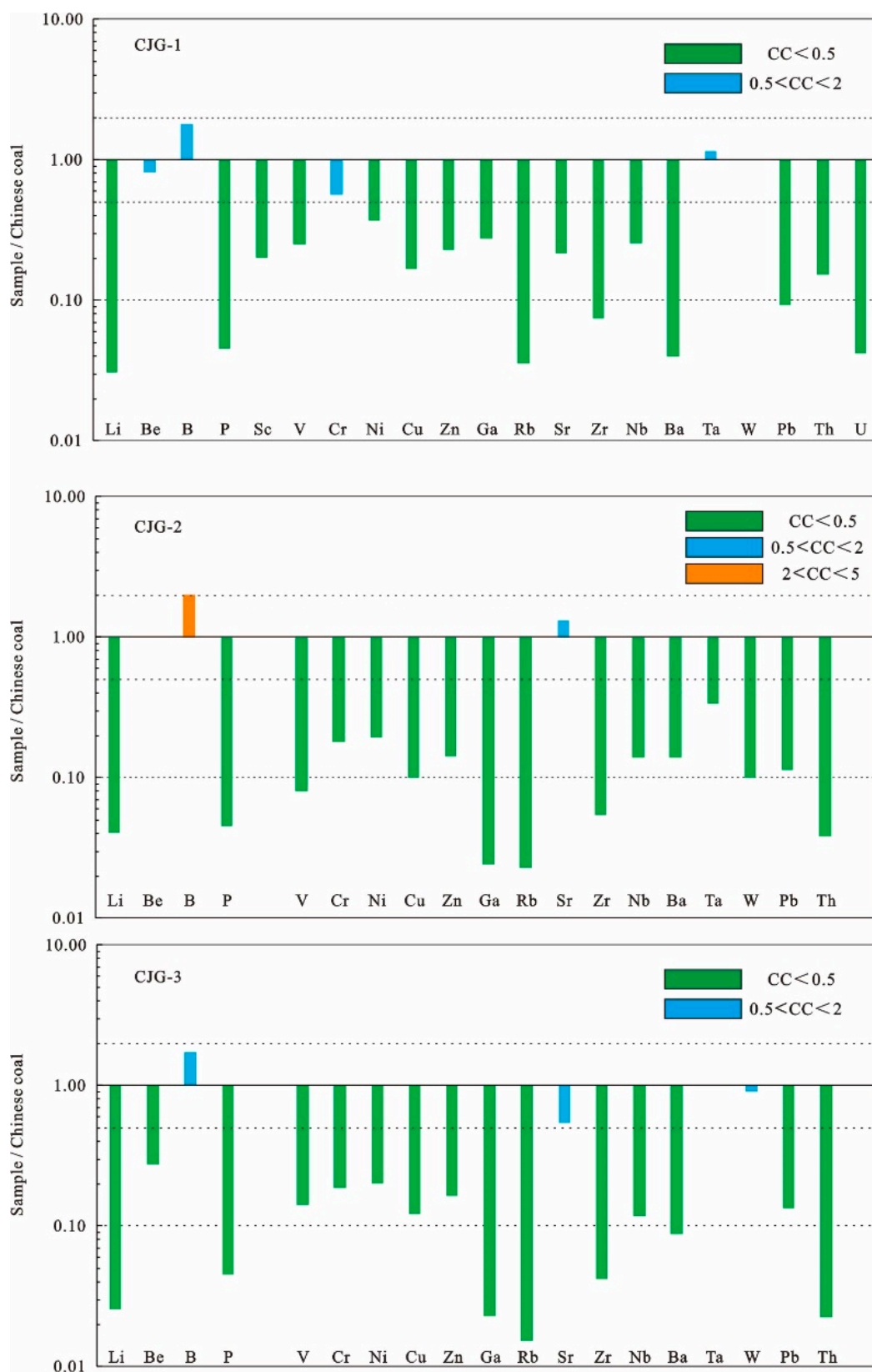


**Figure 10.** Concentration coefficients (CC) of trace elements of the Jurassic coals in the Cuijiagou underground coal mine compared to the averages trace elements for Chinese coals [5].

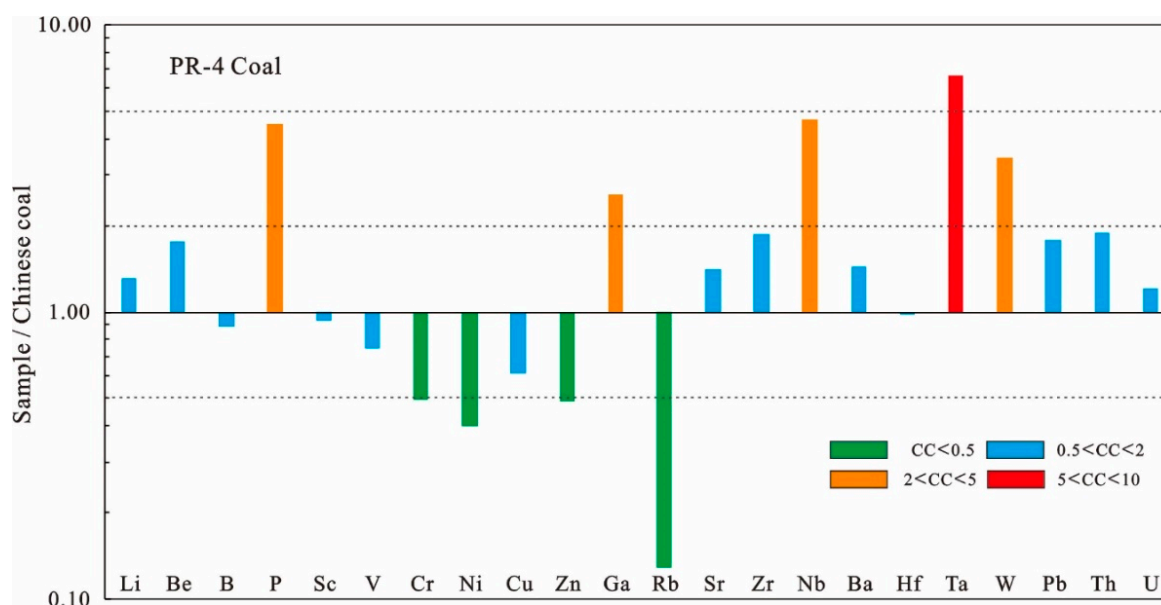


**Figure 11.** Concentration coefficients (CC) of trace elements of the No. 4 coals in the Permian of the Puran coal mine. Normalized by averages of trace elements in the Chinese coals [3].

#### 4.3.2. Rare Earth Elements and Yttrium (REY)

The classification of the REY proposed by Seredin and Dai [57], divided REY into three groups: LREY (La, Ce, Pr, Nd, and Sm), MREY (Eu, Gd, Tb, Dy, and Y), and HREY (Ho, Er, Tm, Yb, and Lu), and three enrichment types (L-type, M-type, and H-type), was used in this study. The REYs concentrations of the Jurassic coals ranged from 1 to 70  $\mu\text{g/g}$  with an average of 29, 6.4, and 8.4  $\mu\text{g/g}$  respectively in No. 1, 2, and 3 coal seams, which is significantly lower than that of Chinese coal (136  $\mu\text{g/g}$ ) [3].

The REY contents of the Permian coals range from 93 to 381  $\mu\text{g/g}$  (189  $\mu\text{g/g}$ , average), slightly higher than that of Chinese coals (136  $\mu\text{g/g}$ , Dai et al. [3]). Furthermore, the parting samples have higher concentrations (367  $\mu\text{g/g}$  on average) than coal samples. The contents of REY increase from the bottom to the top and reach the maximum adjacent to the partings. It is worth noting that the contents of REY in the roof sample are distinctly lower than in adjacent coal immediately below the roof (105 and 219  $\mu\text{g/g}$ , respectively). The Upper Continental Crust (UCC [58])-normalized REY distribution pattern is characterized by an L-type in the partings (PR-4-3, PR-4-4), M-type in the coal sample (PR-4-5), and H-type both in coal and non-coal samples (roof PR-4-T, coal PR-4-1, and parting PR-4-2). In addition, all the samples have moderate negative Eu anomalies (average Eu/Eu\* value of 0.61) (Figure 12), indicating a derivation from felsic composition [6].

#### 4.3.3. Modes of Occurrence of Selected Elements in Coal

There are three modes of occurrence of elements in coals proposed by Dai et al., (2020), i.e., organic, mineral, and intimate organic associations [59]. The organic and intimate organic association were preliminarily identified by evaluating the coefficients of element contents with ash yield for the different coals [60,61]. In order to obtain full interpretation of the relationship, we showed the X-Y plots of selected elements and ash yield (Figures 13 and 14).

In Jurassic No. 1 coal from the Cuijiagou coal mine, MgO shows positive correlation with ash yield ( $r = 0.88$ ), indicating mineral association (Figure 13A). There is no obvious correlation among MgO, CaO and  $\text{Fe}_2\text{O}_3$ , whereas  $\text{SiO}_2$  and  $\text{Al}_2\text{O}_3$  ( $r = 0.86$ , Figure 13B), MgO and  $\text{SiO}_2$  ( $r = 0.79$ ), MgO and  $\text{Al}_2\text{O}_3$  ( $r = 0.77$ ) have significant positive correlations, which is in agreement with the presence of clay minerals such as kaolinite in the coals. In addition, the correlation coefficient of Mn and CaO is 0.97

(Figure 13C), indicating a carbonate association. B and ash yield have negative correlation ship with correlation coefficient  $-0.73$ , indicating that B may has intimate organic association (Figure 13D).

With respect to the elements in No. 2 coal, CaO and ash yield ( $r = 0.91$ ) as well as CaO and MgO ( $r = 0.99$ ) have significantly positive correlation that may be due to the high content of calcite, dolomite, and ankerite in the coals (Figure 13E,F). In addition, Mn has higher correlation coefficient with MgO ( $r = 0.71$ ) indicating a dominant dolomite association (Figure 13G). B has some degree of positive correlation ship with ash yield when we removed some single outlier points ( $r = 0.87$ , Figure 13H) indicating that B may has both inorganic and organic associations.

In No. 3 coal,  $\text{SiO}_2$  and  $\text{Al}_2\text{O}_3$  has a significant positive correlation with ash yield ( $r = 0.98$ , Figure 13I–K) and the correlation coefficients of most of the trace elements with  $\text{SiO}_2$  and  $\text{Al}_2\text{O}_3$  are  $>0.7$ , indicating an aluminosilicate association. B presents slightly negative correlation with ash yield ( $r = -0.62$ , Figure 13L) indicating an intimate organic association.

As for the Permian No. 4 coal, most of the elements have mineral associations ( $r_{\text{ash}} = 0.52\text{--}0.99$ , Figure 14A,B,D–I). As the major clay mineral in the coal samples, kaolinite plays an important role in hosting most of the trace elements, which is confirmed by the correlation coefficients between most elements and  $\text{SiO}_2\text{--Al}_2\text{O}_3$ . Besides, Ca, P, and Sr have strong positive correlation with each other ( $r_{\text{Ca-P}} = 0.74$ ,  $r_{\text{Ca-Sr}} = 0.79$ ,  $r_{\text{P-Sr}} = 0.95$ , Figure 14J–L) which may be caused by abundance of apatite in the coal seam. Some other elements, such as Y, Ba, U, REYs, also have positive correlations with Ca, P, or Sr ( $r > 0.5$ ) indicating an apatite association. Besides, the correlation coefficient of S and ash yield is  $-0.81$  indicating that S occurs in organic matter (Figure 14B).

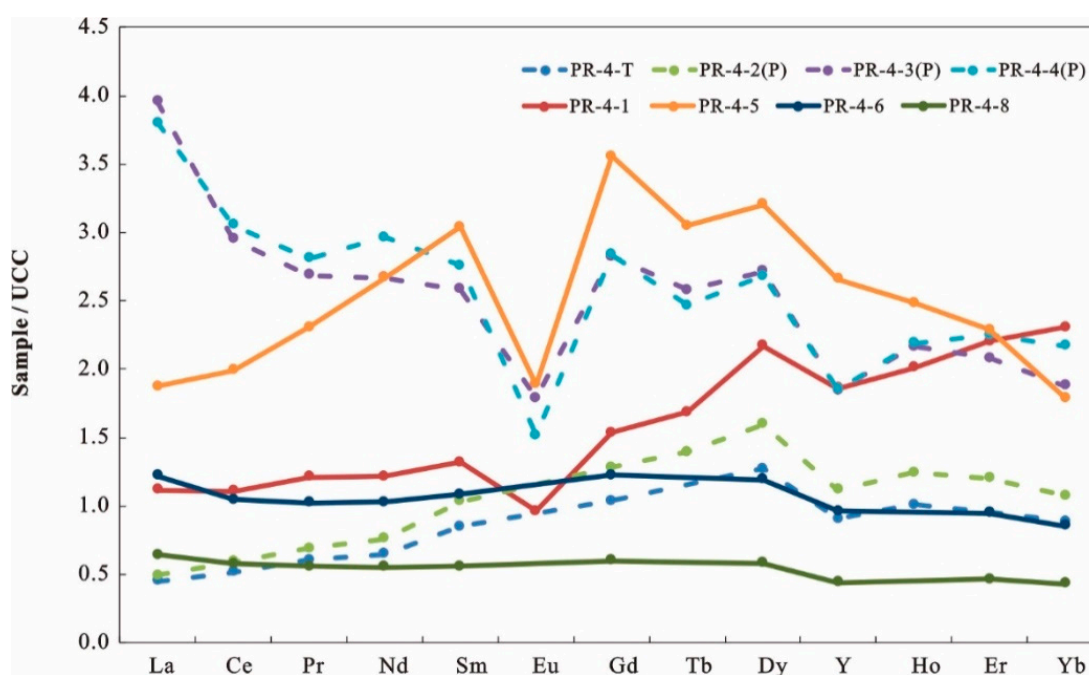


**Figure 12.** The Upper Continental Crust (UCC)-normalized rare earth elements and yttrium (REY) distribution patterns in the Permian coals. (UCC data are from Taylor and McLennan [56]).

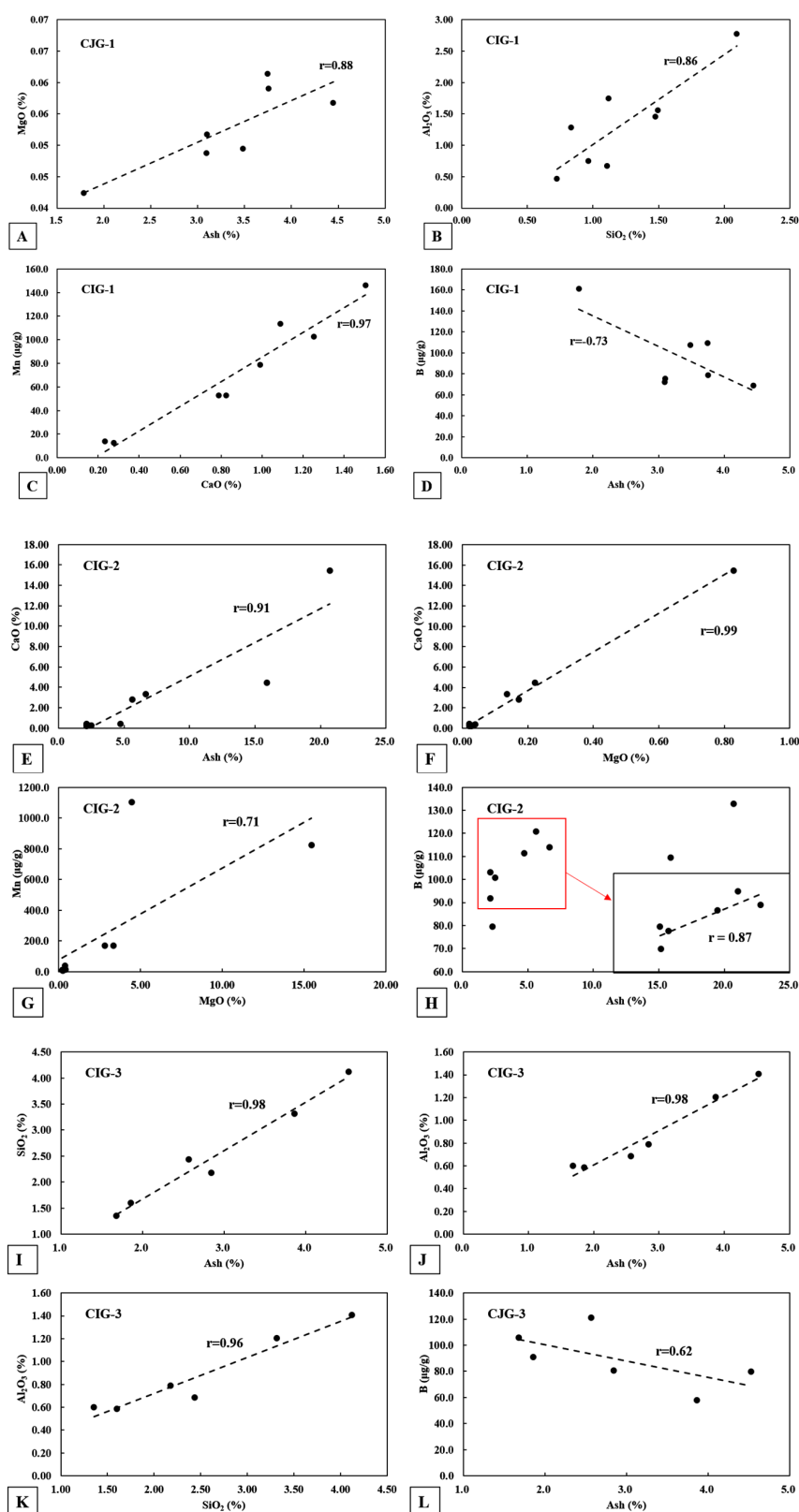


**Figure 13.** Relationship between selected elements/oxide and ash yield in Jurassic coals (CJG-1, 2, 3). CJG-1: (A) MgO-Ash yield; (B)  $Al_2O_3$ - $SiO_2$ ; (C) Mn-CaO; (D) B-Ash yield. CJG-2: (E) CaO-Ash yield; (F) CaO- MgO; (G) Mn-MgO; (H) B-Ash yield. CJG-3: (I)  $SiO_2$ -Ash yield; (J)  $Al_2O_3$ -Ash yield; (K)  $Al_2O_3$ - $SiO_2$ ; (L) B-Ash yield.

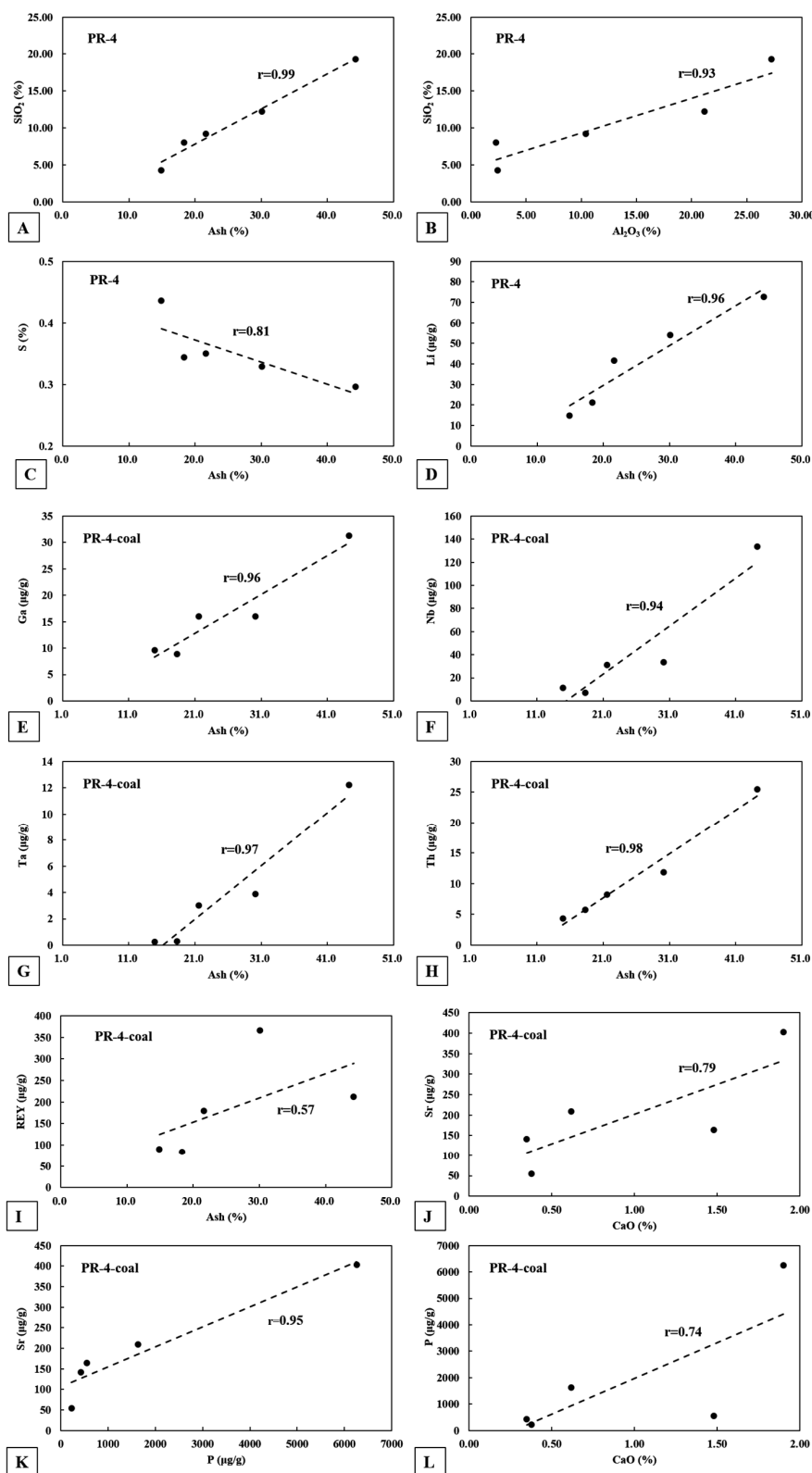


**Figure 14.** Relationship between selected elements/oxide and ash yield in Permian coals/non-coals (PR-4). PR-4: (A)  $SiO_2$ -Ash yield; (B)  $Al_2O_3$ - $SiO_2$ ; (C) S-Ash yield; (D) Li-Ash yield. PR-4-coal: (E) Ga-Ash yield; (F) Nb-Ash yield; (G) Ta-Ash yield; (H) Th-Ash yield; (I) REY-Ash yield; (J) Sr-CaO; (K) Sr-P; (L) P-CaO.

## 5. Discussion

### 5.1. Sedimentary Source Rocks

The sediment source region of coal deposits is generally identified by using geochemical indicators [61–65]. The  $Al_2O_3/TiO_2$  ratio has been proved to be an effective index to reflect the geochemical composition of source rocks due to its stability during sedimentary processes, with ratios of 3–8, 8–21, >21, being respectively indicative of mafic, intermediate, and felsic rocks [65]. All coal samples of this study have higher  $Al_2O_3/TiO_2$  ratios (more than 21), indicating detrital materials with a felsic-dominated composition (Figure 15). In the plot of Th/Sc vs. Zr/Sc (Figure 16) [66], the Permo-Carboniferous coals, including Jungar Coalfield [18–20,67], Daqingshan Coalfield [27,66], Shanbei Coalfield (this study), assembled in the felsic rock zone reflecting the same source rock type. The Jurassic coals, including Dongsheng Coalfield [34] and Shanbei Coalfield (this study), are scattered between the zone of intermediate and felsic rock but more closely to felsic rock (Figure 16).

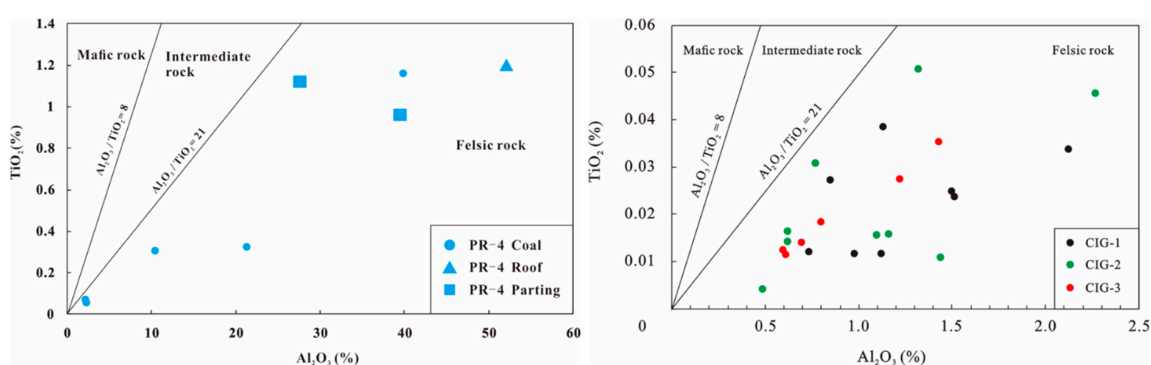


**Figure 15.**  $Al_2O_3$ - $TiO_2$  cross-correlation plot for the Cuijiagou and Puran coals as well as partings and roof.

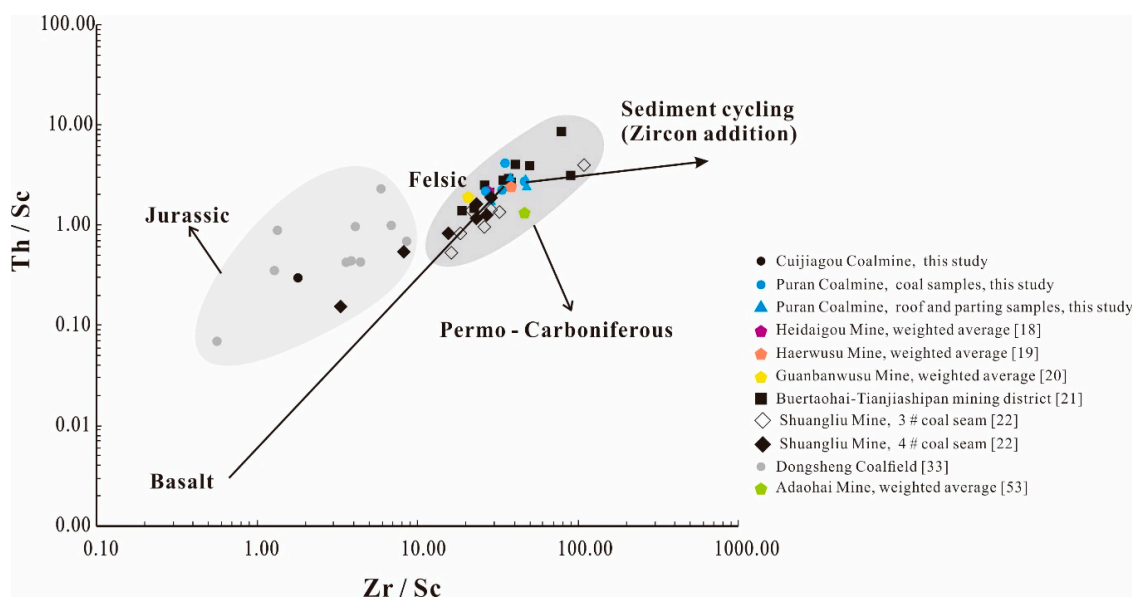


**Figure 16.** Th/Sc-Zr/Sc cross-correlation plot for the Cuijiagou and Puran coals as well as partings and roof, comparing with the Jungar and Daqingshan coals.

The REY distribution patterns and Eu anomalies are also used as important identifications of sedimentary source rocks [6,65]. However, the content of Eu may be interfered with by Ba during ICP-MS analysis [68]. Yang et al., (2018) proposed if  $Ba/Eu > 1000$ , Ba would significantly interfere with Eu [68]. In the present study, the ratio of Ba/Eu range from 148 to 402 (Table 4) indicating that Eu was not interfered by Ba. The felsic volcanic rocks have higher ratios of LREY/HREY and strong negative Eu anomalies, whereas mafic volcanic rocks have low LREE/HREE ratios and no negative Eu anomalies [64,69]. The samples have moderate negative Eu anomalies ( $Eu/Eu^*$ , average 0.61) indicating felsic rocks origin (Table 4), which is in accordance with previous studies that the major sediment-source region of the N China Coal Basin is the Yinshan Oldland, which is made up of felsic rocks [5].

Prior studies reported that there are two different sediment source regions: the Yinshan Oldland (N and W); and the Benxi Formation (N and E) [18,20,29,35]. Boehmite is generally thought to be derived from the weathering crust, and it has two modes of occurrence in the adjacent coalfield: (I) boehmite occurs as massive lumps in collodetrinite and cell infillings of fusinite [18,19,29]; (II) boehmite is also enclosed by kaolinite and occurs as a massive lens which may be derived from the breakdown of kaolinite rather than detrital input or by precipitation from an Al-rich colloidal solution [52]. The mode of occurrence of boehmite in this study is different from that stated above, occurring as finely disseminated impregnations within the kaolinite matrix (Figure 9B), which may be precipitated from Al-rich solution derived from the bauxite of the Benxi Formation.

## 5.2. Diagenetic Fluid Supplies

Hydrothermal fluid (syngenetic and epigenetic) is another important geological controlling factor on the mineralogy and geochemistry of the coal and non-coal samples in this study.

Comparing with the Permian coals, the Jurassic coals, especially No. 1 and 2 coals, have high proportion of carbonate minerals. These minerals mainly occur as a fracture or cleat in-fillings (Figure 5) indicating precipitation from fluids that permeated through the coal along fracture or/and cleat after burial and rank advance [45]. Furthermore, some epigenetic fracture or cleat infilling of kaolinite, was also observed under the SEM-EDS (Figure 5), also providing some evidence for the input of hydrothermal fluids.

With respect to the Permian coals, partings and roof sample, although epigenetic fluids influenced some samples, such as fracture in-filling dolomite in PR-4-6 (Figure 4E), but did not have a noticeable impact on the trace element distribution in the coal seam. Hydrothermal fluid of syngenetic stage played more important role in the enrichment of trace elements. Unlike in the Jurassic coals, kaolinite mainly occurs as cell or pore space infillings which precipitated from fluids derived from weathered source region. Apatite also occurs cell infillings alone or together with kaolinite, indicating the input of syngenetic hydrothermal fluid. Furthermore, sample PR-4-5 is characterized by M-type REY distribution and positive Gd anomaly ( $Gd_N/Gd_N^* = 1.2$ ), indicating the input of hydrothermal fluids as reported by Seredin and Dai [57].

As mentioned above (Section 4.2.2), P was detected in zircon grain (Figures 8A and 9A), and Zr was also detected in apatite grain (Figures 8C and 9C) which may be caused by acid hydrothermal fluid. Generally, Zr are essentially immobile during chemical weathering [70,71], however, under the effect of intense acid hydrothermal fluids, it may become mobilized [28,72]. In this study, during syngenetic to early diagenetic stage, zircon was corroded by acid hydrothermal fluid which eventually precipitated and formed apatite. The coupled substitution of  $REY^{3+} + P^{5+}$  for  $Zr^{4+} + Si^{4+}$  or  $REY^{3+} + (Nb, Ta)^{5+}$  for  $2Zr^{4+}$  in the zircon crystal lattice may cause zircon to contain some P [73].

**Table 4.** Trace elements concentrations ( $\mu\text{g/g}$ , db) in coals and non-coals from the two coal mines (on whole-coal basis). Average concentrations of Chinese coal date from Dai et al., [5].

Sample	Li	Be	B	P	Sc	V	Cr	Ni	Cu	Zn	Ga	Rb	Sr	Y	Zr	Nb	Ba	La
CJG-1-1	1.2	8.6	104	17	5.9	27	35	8.1	3.2	5.7	6.9	<dl	35	25.7	11	5.5	5.3	5.7
CJG-1-2	1.5	<dl	79	18	<dl	3.6	4.2	2.3	<dl	10	0.80	<dl	29	4.4	7	3.1	5.9	4.3
CJG-1-3	1.1	<dl	71	18	<dl	3.5	3.3	2.2	<dl	7.7	<dl	<dl	24	2.4	4.5	1.7	2.5	2.8
CJG-1-4	1.5	<dl	74	17	<dl	3.8	4.1	3.0	1.5	6.4	<dl	<dl	35	1.9	11	3.0	3.6	3.0
CJG-1-5	<dl	<dl	104	19	<dl	5.8	2.9	7.3	1.6	18	<dl	<dl	33	1.4	3.4	0.86	4.5	2.3
CJG-1-6	0.90	<dl	70	20	<dl	4.2	3.1	2.6	1.2	8.0	<dl	<dl	25	1.1	2.4	0.98	2.5	2.3
CJG-1-7	<dl	<dl	154	19	<dl	8.6	5.1	6.7	9.4	9.5	1.0	<dl	25	4.8	7.5	1.7	14	3.5
CJG-1-8	1.6	4.6	114	17	1.1	14	9.7	9.1	7.1	9.8	5.8	2.6	36	21	6.5	2.7	12	7.2
Average	0.98	1.7	96	18	0.88	8.8	8.4	5.2	3.0	9.4	1.8	0.33	30	7.8	6.7	2.4	6.3	3.9
CJG-2-1	1.0	<dl	123	18	<dl	2.5	2.7	2.5	1.7	12	<dl	<dl	160	<dl	3.2	1.1	15	<dl
CJG-2-2	0.84	<dl	134	18	<dl	1.0	1.8	1.9	<dl	4.6	<dl	<dl	323	<dl	1.0	<dl	39	1.0
CJG-2-3	1.5	<dl	114	18	<dl	1.4	2.3	2.1	1.4	4.3	<dl	<dl	145	<dl	1.9	<dl	16	1.3
CJG-2-4	2.0	<dl	113	17	<dl	6.3	4.8	2.7	4.3	7.7	1.4	1.9	224	2.0	11	2.5	25	3.4
CJG-2-5	1.4	<dl	104	19	<dl	2.1	2.9	2.3	2.8	4.4	<dl	<dl	146	2.0	9	3.1	22	2.2
CJG-2-6	0.78	<dl	106	18	<dl	1.8	2.3	3.0	1.5	5.0	<dl	<dl	142	<dl	2.6	0.85	19	<dl
CJG-2-7	1.1	<dl	96	19	<dl	2.0	2.8	2.5	1.9	3.5	<dl	<dl	159	0.85	5.4	2.0	26	1.2
CJG-2-8	1.6	<dl	100	16	<dl	6.1	2.4	3.6	1.6	6.0	<dl	<dl	179	<dl	6.1	1.3	19	2.0
CJG-2-9	1.1	<dl	74	19	<dl	2.1	2.2	3.4	1.4	4.5	<dl	<dl	190	2.0	3.6	1.0	18	2.2
Average	1.3	0	107	18	<dl	2.8	2.7	2.7	1.8	5.8	0.16	0.21	185	0.76	4.9	1.3	22	1.5
CJG-3-1	1.4	1.3	87	16	<dl	4.5	4.2	3.6	4.1	6.2	0.87	0.81	93	5.0	7.1	2.5	20	2.9
CJG-3-2	1.5	<dl	58	18	<dl	3.2	3.3	2.2	2.2	4.9	<dl	<dl	97	1.1	4.7	1.8	17	2.2
CJG-3-3	1.1	<dl	83	17	<dl	4.5	2.6	2.2	2.1	11	<dl	<dl	84	<dl	3.5	1.3	16	1.2
CJG-3-4	<dl	<dl	88	19	<dl	3.8	2.2	1.5	1.4	5.9	<dl	<dl	63	<dl	2.1	<dl	11	<dl
CJG-3-5	<dl	<dl	111	17	<dl	8.0	2.5	3.2	1.7	5.0	<dl	<dl	62	<dl	2.3	<dl	11	1.2
CJG-3-6	0.83	2.2	119	18	<dl	5.1	2.2	4.1	1.5	6.9	<dl	<dl	56	5.0	3.1	1.1	11	2.7
Average	0.81	0.58	91	18	<dl	4.9	2.8	2.8	2.2	6.7	0.15	0.14	76	1.9	3.8	1.1	14	1.7
Chinese coal	32	2.1	53	402	4.4	35	15	14	18	41	6.6	9.3	140	18	90	9.4	159	23

Table 4. Cont.

Sample	Ce	Pr	Nd	Sm	Gd	Dy	Ho	Er	Yb	Ta	W	Pb	Th	U	ΣREY	LREY	MREY	HREY	Ce/Ce*
CJG-1-1	15.1	2.2	11	2.9	3.4	4.9	1.1	3.6	4.0	2.5	1.5	3.6	1.7	<dl	79	37	34	8.7	0.99
CJG-1-2	7.6	0.84	3.4	<dl	<dl	<dl	<dl	<dl	<dl	<dl	1.1	<dl	1.2	<dl	21	16	4.4	<dl	0.93
CJG-1-3	5.0	<dl	2.2	<dl	<dl	<dl	<dl	<dl	<dl	1.0	<dl	<dl	<dl	<dl	12	9.9	2.4	<dl	-
CJG-1-4	4.8	<dl	2.0	<dl	<dl	<dl	<dl	<dl	<dl	<dl	<dl	<dl	1.3	<dl	12	9.7	1.9	<dl	-
CJG-1-5	3.5	<dl	1.6	<dl	<dl	<dl	<dl	<dl	<dl	<dl	0.87	<dl	<dl	<dl	8.8	7.4	1.4	<dl	-
CJG-1-6	3.4	<dl	1.4	<dl	<dl	<dl	<dl	<dl	<dl	0.99	<dl	1.0	<dl	<dl	8.2	7.1	1.1	<dl	-
CJG-1-7	7.6	0.96	3.7	<dl	<dl	<dl	<dl	<dl	<dl	1.0	3.3	2.0	1.1	<dl	21	16	4.8	<dl	0.99
CJG-1-8	17.2	2.3	10	2.4	2.7	3.2	<dl	2.0	1.7	<dl	3.3	3.5	1.7	0.8	70	40	27	3.7	0.98
Average	8	0.79	4.4	0.66	0.76	1.0	0.14	0.7	0.71	0.69	1.1	1.4	0.88	0.10	29	18	9.6	1.5	0.97
CJG-2-1	1.3	<dl	<dl	<dl	<dl	<dl	<dl	<dl	<dl	<dl	<dl	1.6	<dl	<dl	1.3	1.3	<dl	<dl	-
CJG-2-2	1.5	<dl	<dl	<dl	<dl	<dl	<dl	<dl	<dl	0.82	<dl	1.1	<dl	<dl	2.4	2.4	<dl	<dl	-
CJG-2-3	2.1	<dl	0.82	<dl	<dl	<dl	<dl	<dl	<dl	<dl	<dl	1.6	<dl	<dl	4.2	4.2	<dl	<dl	-
CJG-2-4	6.8	<dl	2.6	<dl	<dl	<dl	<dl	<dl	<dl	<dl	<dl	2.6	1.0	<dl	15	12.8	2.1	<dl	-
CJG-2-5	5.1	<dl	2.4	<dl	<dl	<dl	<dl	<dl	<dl	<dl	<dl	1.6	<dl	<dl	12	9.7	2.0	<dl	-
CJG-2-6	1.3	<dl	<dl	<dl	<dl	<dl	<dl	<dl	<dl	1.0	<dl	1.8	<dl	<dl	1.3	1.3	<dl	<dl	-
CJG-2-7	1.9	<dl	0.88	<dl	<dl	<dl	<dl	<dl	<dl	<dl	<dl	1.4	<dl	<dl	4.7	3.9	0.88	<dl	-
CJG-2-8	2.9	<dl	1.1	<dl	<dl	<dl	<dl	<dl	<dl	<dl	<dl	2.1	1.0	<dl	6.0	6.0	<dl	<dl	-
CJG-2-9	4.8	<dl	2.2	<dl	<dl	<dl	<dl	<dl	<dl	<dl	1.0	1.9	<dl	<dl	11	9.3	2.0	<dl	-
Average	3.1	<dl	1.1	<dl	<dl	<dl	<dl	<dl	<dl	0.20	0.11	1.7	0.22	<dl	6.4	5.6	1.7	<dl	-
CJG-3-1	6.3	<dl	3.3	<dl	<dl	<dl	<dl	<dl	<dl	<dl	3.6	3.0	0.78	<dl	17	13	2.9	<dl	-
CJG-3-2	3.5	<dl	1.4	<dl	<dl	<dl	<dl	<dl	<dl	<dl	<dl	1.8	<dl	<dl	8.2	7.1	2.2	<dl	-
CJG-3-3	2.1	<dl	0.83	<dl	<dl	<dl	<dl	<dl	<dl	<dl	<dl	1.6	<dl	<dl	4.2	4.2	1.2	<dl	-
CJG-3-4	1.0	<dl	<dl	<dl	<dl	<dl	<dl	<dl	<dl	<dl	<dl	1.4	<dl	<dl	1.0	1.0	<dl	<dl	-
CJG-3-5	1.9	<dl	0.78	<dl	<dl	<dl	<dl	<dl	<dl	<dl	<dl	2.0	<dl	<dl	3.9	3.9	1.2	<dl	-
CJG-3-6	5.2	<dl	2.7	<dl	<dl	<dl	<dl	<dl	<dl	<dl	2.6	2.4	<dl	<dl	16	11	2.7	<dl	-
Average	3.3	<dl	1.5	<dl	<dl	<dl	<dl	<dl	<dl	<dl	1.0	2.0	0.13	<dl	8.4	6.6	1.7	<dl	-
Chinese coal	47	6.4	22	4.1	4.7	3.7	1.0	1.8	2.1	0.6	1.1	15.1	5.8	2.4	-	-	-	-	-

Table 4. Cont.

Sample	Li	Be	B	P	Sc	V	Cr	Ni	Cu	Zn	Ga	Rb	Sr	Y	Zr	Nb	Ba	La	Ce	Pr	Nd
PR-4-T	171	3.3	34	636	7.8	36	8.5	5.1	11	32	35	2.5	56	20	372	94	77	14	33	4.3	17
PR-4-1	75	9.6	33	227	9.8	44	13	5.8	12	41	32	4	56	41	455	137	229	34	71	8.6	32
PR-4-2(P)	167	3.6	35	545	9.2	40	10	5.7	12	34	36	3	58	25	433	96	84	15	37.9	4.9	20
PR-4-3(P)	177	6.4	33	1850	15	55	23	9.7	21	28	37	25	626	41	431	99	232	119	188.8	19	69
PR-4-4(P)	159	6.5	42	3381	12	38	17	7.7	11	32	33	3.9	762	41	444	211	354	114	195.5	20	77
PR-4-5	56	4.2	42	6256	5.7	27	9.9	6.8	13	15	17	1.8	420	59	153	35	668	56	127.4	16	69
PR-4-6	41	2	44	1632	3.8	30	7.7	7.1	11	17	16	<dl	207	21	127	31	175	37	66.9	7.3	27
PR-4-7	20	1.5	53	426	1.3	17	4.1	4.4	14	13	8.2	<dl	130	6.5	46	6.4	36	17	31.2	3.3	12
PR-4-8	16	1.4	64	551	<dl	13	2.5	4.1	7.4	12	10	<dl	173	9.7	59	12	41	19	36.9	4.0	14
Average (coal)	42	3.7	47	1818	4.1	26	7.4	5.6	11	20	17	1.2	197	27	168	44	230	33	67	7.8	31
Chinese coal	32	2.1	53	402	4.4	35	15	14	18	41	6.6	9.3	140	18	90	9.4	159	23	47	6.4	22
sample	Sm	Eu	Gd	Tb	Dy	Ho	Er	Yb	Hf	Ta	W	Pb	Th	U	ΣREY	LREY	MREY	HREY	Ba/Eu	Eu/Eu*	Ce/Ce*
PR-4-T	3.8	<dl	3.9	<dl	4.4	0.84	2.2	2.0	8.3	8.1	10.4	36	19	7.1	105	71	28	5.0	-	-	0.99
PR-4-1	5.9	0.82	5.8	1.1	7.6	1.6	5.1	5.1	9.3	13	9.7	49	26	3.4	219	151	56	12	269	0.68	0.95
PR-4-2(P)	4.6	<dl	4.9	0.86	5.6	1.0	2.8	2.4	10	6.9	9.8	41	25	7.3	124	82	36	6.1	-	-	1.02
PR-4-3(P)	12	1.6	11	1.7	9.5	1.7	4.8	4.1	9.5	9.3	10	39	26	5.0	482	407	64	11	148	0.66	0.91
PR-4-4(P)	12	1.3	11	1.6	9.4	1.8	5.2	4.8	11	22	10.8	38	35	5.8	494	419	64	12	265	0.54	0.93
PR-4-5	14	1.7	14	2.0	11	2.0	5.3	3.9	3.5	4.0	3.3	28	12	5.8	381	283	87	11	402	0.57	0.96
PR-4-6	4.9	<dl	4.7	<dl	4.2	<dl	2.2	1.9	2.9	3.0	2.9	20	8.2	3.3	177	142	30	4.1	-	-	0.94
PR-4-7	2.0	<dl	1.7	<dl	1.4	<dl	<dl	<dl	1.1	<dl	1.0	24	5.3	1.2	75	66	9.7	<dl	-	-	0.94
PR-4-8	2.5	<dl	2.3	<dl	2.0	<dl	1.1	0.90	1.3	<dl	2.1	13	4.5	1.0	93	77	14	2.0	-	-	0.97
Average (coal)	5.9	0.50	5.7	0.62	5.2	0.72	2.7	2.4	3.6	4.0	3.8	27	11	2.9	189	144	39	5.8	-	0.63	0.95
Chinese coal	4.1	0.8	4.7	0.6	3.7	1	1.8	2.1	3.7	0.6	1.1	15.1	5.8	2.4	-	-	-	-	-	-	-

db-dry basis; &lt;dl, below detection limit.

### 5.3. Enrichment of Trace Elements

#### 5.3.1. Boron

The ash yield is approximately 10 times lower in the Jurassic than in the Permian coals but the B contents are approximately 2 times higher in the Jurassic ones. Boron has organic association in the Permian coals ( $r_{\text{ash}} = -0.93$ ), and both organic (No. 1 and 3 coals with  $r_{\text{ash}} = -0.73, -0.62$ ) and inorganic association (No. 2 coals with  $r_{\text{ash}} = 0.87$ ) in the Jurassic coals. Calcite, as a primary mineral in the No. 2 coal, has significant positive correlation with B ( $r_{\text{cal-B}} = 0.97$ ). This differs markedly to previous studies where B is inorganic association was closely related with clay minerals (especially illite) or tourmaline [74–77].

In general, B concentrations are closely related to the paleo-salinity of the depositional water. The coals deposited in the marine-influenced environments, such as tidal flat environments of restricted carbonate platforms [5,19,78,79], and some non-marine-influenced environments such as brackish peat formed in the distributary channel–delta front, beach bar and interdistributary bay [24], are enriched in B. In addition, hydrothermal fluids, volcanic activity, acidic water, and climatic variation also elevated the concentration of B [80–87].

Previous studies showed that the Permian Shanxi Formation coals were deposited in the fluvial and deltaic environments [35,88] and the No. 1 and 3 coals of the Jurassic Yan'an Formation were deposited in the lake delta plain [37,89]. However, the indicator of Sr/Ba, which is a useful indicator for climatic conditions with  $>1$  for arid and  $<1$  for humid [90,91], is different between the Jurassic and Permian coals. The average ratios of Sr/Ba in the Jurassic coals are 4.7 (No. 1), 8.6 (No. 2), and 5.3 (No. 3) whereas in the Permian coal it is 1.2 indicating a more arid climate. The climatic variation may be one of the reasons caused enrichment of B in the Jurassic coals.

On the other hand, as mentioned above, B has organic associations, suggesting that the elevated concentration of B may be absorbed by organic matter from fluid (or groundwater) or inherited from coal-forming plants as evidenced by the boron content being higher in the lower ash-yield coals [89]. According to Wang (1996) the dominant coal-forming plants of the Late Paleozoic are herbaceous vegetation (90.1%) which is mainly fern, whereas the Jurassic Yan'an Formation are both woody plants (66.9%) and herbaceous vegetation [35]. The different types of coal-forming plants might result in the different B contents between the Jurassic and Permian coals.

#### 5.3.2. Phosphorus, Sr, and Ba

Comparing with adjacent coalfields, the Permian coals in the Puran coal mine have higher contents of P in both coals (1818  $\mu\text{g/g}$ , average) and non-coal rocks (1603  $\mu\text{g/g}$ , average), especially in the coal sample of PR-4-5 (6256  $\mu\text{g/g}$ ), approximately 15 times higher than the average of common Chinese coals (402  $\mu\text{g/g}$ ) [5]. Phosphorous was concentrated in the samples where apatite was detected. The strong positively correlation between P and CaO ( $r = 0.74$ ) also indicates that P is mainly incorporated into apatite. In addition, P and Sr ( $r = 0.96$ ), P and Ba ( $r = 0.94$ ) have significant positive correlations, which is in accordance with the Heidaigou [18], Haerwusu [19], and Buertanhai–Tianjiashipan [21] coals. In these coalfields, the major carrier of P is goyazite (Haerwusu and Heidaigou coals) and svanbergite (Buertanhai–Tianjiashipan coals) [18–21]. However, these minerals are neither detected by XRD nor by SEM-EDS in this study. Accordingly, Sr and Ba probably occur in apatite. Besides, P and REYs also have a good positive correlation ( $r = 0.87$ ) indicating apatite as the host of REYs. Furthermore, Nb and Y were detected in apatite by means of SEM-EDS (Figure 8C). This mode of occurrence of REYs is different from P-bearing minerals (goyazite and svanbergite) in the Junger Coalfield coals [19,21].

In the present study, almost all apatite shows syngenetic origin, which may derive from volcanic input [45,90] or to the supply of Ca- and Al-rich solutions combined with P which was released from the decay of organic matter in a suitable geochemical setting [92], and non-fracture filling apatite (epigenetic origin), was identified by SEM-EDS. Dai et al., (2017) distinguished authigenic apatite from

volcanic apatite based on the mode of occurrence [93]. Generally, volcanic apatite “occurs as euhedral and elongate hexagonal grains, and can contain distinctive fluid inclusions, in some cases, the delicate and elongate apatite grains may have fractured as a result of compaction, or have been altered [93]”, which obviously is different from present study.

The Al-rich solution arising from the weathering of bauxite (Benxi Formation) yielded to mineral precipitation under a higher pH environment to initially form aluminum hydroxide mineral (gibbsite and boehmite). In general, gibbsite is unstable in the presence of SiO<sub>2</sub>, and if SiO<sub>2</sub> is available, authigenic kaolinite precipitation might be favored [45]. With respect to apatite, it has also been detected in the Adaohai mine and was also affected by input of diagenetic solution from bauxite contained in the Benxi Formation [53]. In this study, authigenic apatite occurs always intimately enclosed or surrounded by kaolinite or organic matter (Figure 6E,F), indicating that apatite precipitated from Al-, Si-, Ca-, and P-rich solutions during syngenetic to early diagenetic stages. This occurrence of apatite is similar to that described elsewhere for coals from the Muli Coalfield on the Tibetan Plateau [93].

### 5.3.3. Niobium, Ta, Ga, and Th

The concentrations of Nb and Ta in the Permian coal samples, respectively range from 7 to 133 µg/g (43 µg/g, average), and from <0.1 to 12 µg/g (7 µg/g, average). Gallium and Th are enriched in different coal mine of the Junger and Daqingshan Coalfields in varying degrees [19–21,53] and are similar to the Daqingshan Coalfield in No. 4 coal, but lower than that of Junger Coalfield, especially Ga. However, the associated non-coal samples are enriched in a number of elements including Li (163 µg/g), Pb (37 µg/g), Ti (6272 µg/g), Sr (352 µg/g), and U (6 µg/g).

The correlation coefficients of Nb and Ta with ash yield ( $r_{\text{Nb-Ash}} = 0.94$ ,  $r_{\text{Ta-Ash}} = 0.94$ ) and kaolinite ( $r_{\text{Nb-Kal}} = 0.93$ ,  $r_{\text{Ta-Kal}} = 0.96$ ) demonstrate a major kaolinite association. Moreover, some Nb and Ta also occur in heavy mineral (zircon, anatase), as evidenced by SEM-EDS (Figure 8A,B and Figure 9A). With respect to the parting samples, Nb and Ta are negatively correlated with ash yield, but positively with Ca and P, suggesting that apatite is the predominant carrier of Nb and Ta in parting samples. This is also further confirmed by the SEM-EDS mappings where Nb has a similar distribution with P within apatite and with Zr in the zircon (Figure 8A,C).

According to previous studies, the elevated contents of Ga in the Junger and Daqingshan Coalfield mainly occurs in aluminosilicate mineral (kaolinite), aluminum hydroxide mineral (boehmite, diaspore, goyazite), and svanbergite [18–21,53], and Th in boehmite, clay minerals, accessory minerals such as zircon, and organic matter [20]. In No. 4 coals, both Ga and Th have aluminosilicate association, as evidenced by the significant correlation with Al<sub>2</sub>O<sub>3</sub> and SiO<sub>2</sub> (Al<sub>2</sub>O<sub>3</sub>:  $r_{\text{Ga}} = 0.91$ ,  $r_{\text{Th}} = 0.92$ ; SiO<sub>2</sub>:  $r_{\text{Ga}} = 0.94$ ,  $r_{\text{Th}} = 0.97$ ), specifically with kaolinite ( $r = 0.94, 0.98$ ). In addition, Th intimately correlated with Ti ( $r = 0.99$ ) and Zr ( $r = 0.99$ ), which also shows that some accessory minerals (e.g., zircon, rutile) may contribute to some proportions of Th in the coal samples. The heavy minerals in the bauxite of Benxi Formation in the north China, one of the main sediment source rocks, are mainly zircon, rutile, and galena [18]. Meanwhile, the other source rocks, the Middle Proterozoic moyite of the Yinshan Oldland also provides a relatively high background value of Th [53]. In the non-coal samples, the correlation analysis shows Ga occurs in kaolinite and Th may occur in apatite ( $r_{\text{Th-CaO}} = 0.89$ ,  $r_{\text{Th-P}} = 0.88$ ).

### 5.3.4. Rare Earth Elements and Y

In the adjacent coalfield, LREY, MREY, and HREY have different degrees of organic matter association in different coal mines. In the Haerwusu coal mine, LREEs have a stronger organic matter association than the HREEs, whereas the opposite was found for the Adaohai coal mine [19,53]. Furthermore, in the Guanbanwusu coal mine, all REYs have similar organic matter association [20]. As for the Puran coal mine, REYs in coals, including LREY, MREY, and HREY, were found with a similar high correlation with ash yield ( $r = 0.91–0.96$ ), suggesting a similar inorganic association.

Finkelman et al., (2019) proposed that in bituminous coals, the bulk (>50%) of all elements except Br were associated with minerals, such as clays, phosphate, and carbonate minerals [94]. Different from the Guanbanwusu coal mine in which LREY are retained in the goyazite, and MREY and HREY occur both in boehmite and accessory minerals, the REYs of the Permian coals have multiple mineral affinities, as evidenced by the positive correlation of REY with kaolinite ( $r = 0.54$ ), and the SEM-EDS mappings showing that zircon, apatite, and boehmite contains Nb and Y (Figure 9).

There are four genetic types of REY enrichment in the coal basin including (I) terrigenous; (II) tuffaceous; (III) infiltrational or meteoric groundwater driven; and (IV) hydrothermal types [57]. Different REY distribution patterns (L-type, M-type, and H-type) indicate different genetic types in coals [20,29,57]. In the Permian coals, REY are mainly enriched in some benches with sample PR-4-1 with H-type distribution, PR-4-5 with M-type, as well as PR-4-6, PR4-3, and PR4-4 with L-type distributions (Figure 12). The L-type REY distribution, in accordance with the Guanbanwusu, Heidaigou, and Haerwusu coals, may be caused by REY-rich colloidal input from the weathered bauxite of the Benxi Formation [18–20].

The uppermost coal sample PR-4-1 is characterized by H-type enrichment which may be affected by stronger groundwater leaching than the other coal samples [20]. Comparing with the middle and bottom parting samples (PR-4-3 and PR-4-4), the upper parting sample PR-4-2 has lower contents of REY, lower ratio of LREY/HREY and  $La_N/Yb_N$ , which was probably caused by the leaching of groundwater. The LREY are more readily leached by ground water than the HREYs, leads to HREYs enrichment in the PR-4-2 but LREYs enrichment in the PR-4-3 and PR-4-4. However, coal samples in the lower portion (especially PR-4-5) have lower contents of REYs (381 vs. 494  $\mu\text{g/g}$ ), lower ratio of LREY/HREY (25 vs. 36), and lower ratio of  $La_N / Yb_N$  (1.05 vs. 1.75) than the overlying parting, which may not be effected by groundwater leaching. The coal sample PR-4-5 is the only one that is characterized by an M-type REY enrichment, which was also identified in the Hailiushu mine by [29], probably indicating the input of a REY-bearing acid hydrothermal solution [29,57].

## 6. Conclusion

The Jurassic and Permian coals have similar chemical characteristics excluding ash yield, which is significantly higher in the Permian coals. The Jurassic coals have relatively lower amounts of mineral matter, which mainly consist of quartz, kaolinite, and calcite while the Permian coals are dominated by kaolinite. Apatite is detected in the partings and coals close to partings, and calcite occurs in the bottom portion of the coal seam. Compared to Chinese coals, the Jurassic coals enriched in B, the Permian coals enriched P, Nb, Ta, Zr, Ga, W, Th and REY.

Previous studies have indicated the Jurassic and Permian coals are formed in similar sedimentary environment and similar B content would be expected, however, the Jurassic coals contain much higher B than the Permian ones. The discrepancy is possibly due to (1) the climatic variation. From the Permian to Jurassic, the climate has become more arid evidenced by increasing ratio of Sr/Ba; (2) B has significant organic matter association indicating the elevated concentration of B may be absorbed by organic matter from fluid (or groundwater) or inherited from coal-forming plants.

In the Permian coals, the sedimentary source rocks dominantly controlled the enrichment of trace elements. Most of the elevated elements, such as Nb, Ta, Ga, Th, have kaolinite association which was derived from weathering of sedimentary source region. Some other elements, P, Sr and Ba, have apatite associations which may be derived from the bauxite on the weathered basement (Benxi Formation) in the sediment source region. Furthermore, REY enrichment is found to be both controlled by ground water and acid hydrothermal fluid based on the genetic types of REY.

Although the present study provides new data of coal mineralogy and geochemistry in the northeastern of Ordos and discussed geological controls about enrichment of some trace elements, there is still an absence of systematic research in temporal and spatial distributions and modes of occurrence of critical elements which need further study.

**Author Contributions:** Conceptualization, Y.S., X.Z., J.L. and B.L. (Baoqing Li); methodology, Y.S., B.L. (Bo Liu) and N.M.; formal analysis, Y.S.; investigation, Y.S., W.Y., B.L. (Baoqing Li); resources, X.Z., G.Y., L.P.; data curation, Y.S., N.M.; writing—original draft preparation, Y.S.; writing—review and editing, Y.S., X.Z., J.L., B.L. (Baoqing Li) and X.Q.; supervision, X.Z., J.L., B.L. (Baoqing Li) and X.Q.; project administration, X.Z., J.L., B.L. (Baoqing Li) and X.Q.; funding acquisition, X.Z., J.L., B.L. (Baoqing Li) and X.Q. All authors have read and agreed to the published version of the manuscript.

**Funding:** This research was funded by the National Science Foundation of China (Nos. 41972179, 41972180), the National Key R&D Program of China (No. 2018YFF0215400), the Fundamental Research Funds for the Central Universities, China University of Geosciences (Wuhan) (No. CUGCJ1823), the “Overseas Top Scholars Program”, part of the “Recruitment Program of Global Experts” (No. G20190017067), and the Open Research Fund Project for Key Laboratory of Tectonics and Petroleum Resources (China University of Geosciences), Ministry of Education (No. TPR-2019-14).

**Conflicts of Interest:** The authors declare no conflict of interest.

## References

- Zhuang, X.; Querol, X.; Alastuey, A.; Juan, R.; Plana, F.; Lopez-Soler, A.; Du, G.; Martynov, V.V. Geochemistry and mineralogy of the Cretaceous Wulantuga higher-germanium coal deposit in Shengli coal field, Inner Mongolia, Northeastern China. *Int. J. Coal Geol.* **2006**, *66*, 119–136. [[CrossRef](#)]
- Zhuang, X.; Querol, X.; Alastuey, A.; Plana, F.; Moreno, N.; Andrés, J.M.; Wang, J. Mineralogy and geochemistry of the coals from the Chongqing and Southeast Hubei coal mining districts, South China. *Int. J. Coal Geol.* **2007**, *71*, 263–275. [[CrossRef](#)]
- Dai, S.; Zhao, L.; Peng, S.; Chou, C.L.; Wang, X.; Zhang, Y.; Li, D.; Sun, Y. Abundances and distribution of minerals and elements in high-alumina coal fly ash from the Jungar power plant, Inner Mongolia, China. *Int. J. Coal Geol.* **2010**, *81*, 320–332. [[CrossRef](#)]
- Dai, S.; Zhou, Y.; Zhang, M.; Wang, X.; Wang, J.; Song, X.; Jiang, Y.; Luo, Y.; Song, Z.; Yang, Z.; et al. A new type of Nb(Ta)–Zr(Hf)–REE–Ga polymetallic deposit in the late Permian coal-bearing strata, eastern Yunnan, Southwestern China: Possible economic significance and genetic implications. *Int. J. Coal Geol.* **2010**, *83*, 55–63. [[CrossRef](#)]
- Dai, S.; Ren, D.; Chou, C.-L.; Finkelman, R.B.; Seredin, V.V.; Zhou, Y. Geochemistry of trace elements in Chinese coals: A review of abundances, genetic types, impacts on human health, and industrial utilization. *Int. J. Coal Geol.* **2012**, *94*, 3–21. [[CrossRef](#)]
- Dai, S.; Graham, I.; Ward, C. A review of anomalous rare earth elements and yttrium in coal. *Int. J. Coal Geol.* **2016**, *159*, 82–95. [[CrossRef](#)]
- Dai, S.; Finkelman, R.B. Coal as a promising source of critical elements: Progress and future prospects. *Int. J. Coal Geol.* **2018**, *186*, 155–164. [[CrossRef](#)]
- Wang, Z.; Dai, S.; Zou, J.; French, D.; Graham, I.T. Rare earth elements and yttrium in coal ash from the Luzhou power plant in Sichuan, Southwest China: Concentration, characterization and optimized extraction. *Int. J. Coal Geol.* **2019**, *203*, 1–14. [[CrossRef](#)]
- Qi, H.; Hu, R.; Zhang, Q. Concentration and distribution of trace elements in lignite from the Shengli Coalfield, Inner Mongolia, China: Implications on origin of the associated Wulantuga Germanium Deposit. *Int. J. Coal Geol.* **2007**, *71*, 129–152. [[CrossRef](#)]
- Hu, R.; Qi, H.; Zhou, M.; Su, W.; Bi, X.; Peng, J.; Zhong, H. Geological and geochemical constraints on the origin of the giant Lincang coal seam-hosted germanium deposit, Yunnan, SW China: A review. *Ore Geol. Rev.* **2009**, *36*, 221–234. [[CrossRef](#)]
- Dai, S.; Wang, P.; Ward, C.R.; Tang, Y.; Song, X.; Jiang, J.; Hower, J.C.; Li, T.; Seredin, V.V.; Wagner, N.J.; et al. Elemental and mineralogical anomalies in the coal-hosted Ge ore deposit of Lincang, Yunnan, southwestern China: Key role of N<sub>2</sub>–CO<sub>2</sub>-mixed hydrothermal solutions. *Int. J. Coal Geol.* **2015**, *152*, 19–46. [[CrossRef](#)]
- Du, G.; Zhuang, X.; Querol, X.; Izquierdo, M.; Alastuey, A.; Moreno, T.; Font, O. Ge distribution in the Wulantuga high-germanium coal deposit in the Shengli coalfield, Inner Mongolia, northeastern China. *Int. J. Coal Geol.* **2009**, *78*, 16–26. [[CrossRef](#)]
- Seredin, V.V.; Danilcheva, J. Coal-hosted Ge deposits of the Russian Far East. In *Mineral Deposits at the Beginning of the 21st Century*; Swets and Zeitlinger Publishers: Lisse, The Netherlands, 2001; pp. 89–92.
- Seredin, V.V.; Danilcheva, Y.A.; Magazina, L.O.; Sharova, I.G. Ge-bearing coals of the Luzanovka Graben, Pavlovka brown coal deposit, southern Primorye. *Lithol. Miner. Resour.* **2006**, *41*, 280–301. [[CrossRef](#)]

15. Dai, S.; Yang, J.; Ward, C.R.; Hower, J.C.; Liu, H.; Garrison, T.M.; French, D.; O'Keefe, J.M.K. Geochemical and mineralogical evidence for a coal-hosted uranium deposit in the Yili Basin, Xinjiang, northwestern China. *Ore Geol. Rev.* **2015**, *70*, 1–30. [[CrossRef](#)]
16. Dai, S.; Seredin, V.V.; Ward, C.R.; Hower, J.C.; Xing, Y.; Zhang, W.; Song, W.; Wang, P. Enrichment of U–Se–Mo–Re–V in coals preserved within marine carbonate successions: Geochemical and mineralogical data from the Late Permian Guiding Coalfield, Guizhou, China. *Mineral. Depos.* **2015**, *50*, 159–186. [[CrossRef](#)]
17. Dai, S.; Xie, P.; Jia, S.; Ward, C.R.; Hower, J.C.; Yan, X.; French, D. Enrichment of U–Re–V–Cr–Se and rare earth elements in the Late Permian coals of the Moxinpo Coalfield, Chongqing, China: Genetic implications from geochemical and mineralogical data. *Ore Geol. Rev.* **2017**, *80*, 1–17. [[CrossRef](#)]
18. Dai, S.; Ren, D.; Chou, C.-L.; Li, S.; Jiang, Y. Mineralogy and geochemistry of the No. 6 coal (Pennsylvanian) in the Jungar coalfield, Ordos Basin, China. *Int. J. Coal Geol.* **2006**, *66*, 253–270. [[CrossRef](#)]
19. Dai, S.; Li, D.; Chou, C.-L.; Zhao, L.; Zhang, Y.; Ren, D.; Ma, Y.; Sun, Y. Mineralogy and geochemistry of boehmite-rich coals: New insights from the Haerwusu surface mine, Jungar coalfield, Inner Mongolia, China. *Int. J. Coal Geol.* **2008**, *74*, 185–202. [[CrossRef](#)]
20. Dai, S.; Jiang, Y.; Ward, C.R.; Gu, L.; Seredin, V.V.; Liu, H.; Zhou, D.; Wang, X.; Sun, Y.; Zou, J.; et al. Mineralogical and geochemical compositions of the coal in the Guanbanwusu Mine, Inner Mongolia, China: Further evidence for the existence of an Al (Ga and REE) ore deposit in the Jungar Coalfield. *Int. J. Coal Geol.* **2012**, *98*, 10–40. [[CrossRef](#)]
21. Li, J.; Zhuang, X.; Yuan, W.; Liu, B.; Querol, X.; Font, O.; Moreno, N.; Li, J.; Gang, T.; Liang, G. Mineral composition and geochemical characteristics of the Li–Ga-rich coals in the Buertaohai–Tianjiashipan mining district, Jungar Coalfield, Inner Mongolia. *Int. J. Coal Geol.* **2016**, *167*, 157–175. [[CrossRef](#)]
22. Yang, N.; Tang, S.; Zhang, S.; Xi, Z.; Li, J.; Yuan, Y.; Guo, Y. In seam variation of element-oxides and trace elements in coal from the eastern Ordos Basin, China. *Int. J. Coal Geol.* **2018**, *197*, 31–41. [[CrossRef](#)]
23. Ren, D.; Zhao, F.; Wang, Y.; Yang, S. Distribution of minor and trace elements in Chinese coals. *Int. J. Coal Geol.* **1999**, *40*, 109–118. [[CrossRef](#)]
24. Ren, D.; Zhao, F.; Dai, S.; Zhang, J.; Luo, K. *Geochemistry of Trace Elements in Coal*; Science Press: Beijing, China, 2006; 556p. (In Chinese)
25. Bouška, V.; Pešek, J.; Sýkorová, I. Probable modes of occurrence of chemical elements in coal. *Acta Montana. Serie B Fuel Carbon Miner. Process. Praha* **2000**, *10*, 53–90.
26. Dai, S.; Ren, D.; Hou, X.; Shao, L. Geochemical and mineralogical anomalies of the late Permian coal in the Zhijin coalfield of southwest China and their volcanic origin. *Int. J. Coal Geol.* **2003**, *55*, 117–138. [[CrossRef](#)]
27. Dai, S.; Ren, D.; Zhou, Y.; Chou, C.-L.; Wang, X.; Zhao, L.; Zhu, X. Mineralogy and geochemistry of a superhigh-organic-sulfur coal, Yanshan Coalfield, Yunnan, China: Evidence for a volcanic ash component and influence by submarine exhalation. *Chem. Geol.* **2008**, *255*, 182–194. [[CrossRef](#)]
28. Dai, S.; Zhang, W.; Ward, C.R.; Seredin, V.V.; Hower, J.C.; Li, X.; Song, W.; Wang, X.; Kang, H.; Zheng, L.; et al. Mineralogical and geochemical anomalies of late Permian coals from the Fusui Coalfield, Guangxi Province, southern China: Influences of terrigenous materials and hydrothermal fluids. *Int. J. Coal* **2013**, *105*, 60–84. [[CrossRef](#)]
29. Dai, S.; Li, T.; Jiang, Y.; Ward, C.R.; Hower, J.C.; Sun, J.; Liu, J.; Song, H.; Wei, J.; Li, Q.; et al. Mineralogical and geochemical compositions of the Pennsylvanian coal in the Hailiushu Mine, Daqingshan Coalfield, Inner Mongolia, China: Implications of sediment-source region and acid hydrothermal solutions. *Int. J. Coal* **2015**, *137*, 92–110. [[CrossRef](#)]
30. Zhao, F.; Cong, Z.; Peng, S.; Tang, Y.; Ren, D. Geochemical characteristics of REE in Jurassic coal of Yan'an formation from Dongsheng coalfield. *J. China. Univ. Min. Technol.* **2002**, *12*, 138–142. (In English)
31. Liu, D.; Zhou, A.; Liu, J. Geochemical characteristics of rare earth elements in Yan'an formation, Jurassic system, Dongsheng coalfield. *Coal Geol. China* **2007**, *19*, 20–22. (In Chinese)
32. Wang, S.M. Ordos basin tectonic evolution and structural control of coal. *Geol. Bull. China* **2011**, *30*, 544–552. (In Chinese)
33. Wang, X.; Jiao, Y.; Wu, L.; Rong, H.; Wang, X.; Song, J. Rare earth element geochemistry and fractionation in Jurassic coal from Dongsheng–Shenmu area, Ordos Basin. *Fuel* **2014**, *136*, 233–239. [[CrossRef](#)]
34. Wang, X.; Wang, X.; Pan, S.; Yang, Q.; Hou, S.; Jiao, Y.; Zhang, W. Occurrence of analcime in the middle Jurassic coal from the Dongsheng Coalfield, northeastern Ordos Basin, China. *Int. J. Coal Geol.* **2018**, *196*, 126–138. [[CrossRef](#)]

35. Wang, S. *Coal Accumulation and Coal Resource Evaluation of Ordos Basin*; China Coal Industry Publishing House: Beijing, China, 1996.
36. Wang, D.; Shao, L.; Li, Z.; Li, M.; Lv, D.; Liu, H. Hydrocarbon generation characteristics, reserving performance and preservation conditions of continental coal measure shale gas: A case study of Mid-Jurassic shale gas in the Yan'an Formation, Ordos Basin. *J. Pet. Sci. Eng.* **2016**, *145*, 609–628. [[CrossRef](#)]
37. ASTM D3173/D3173M-17a, *Standard Test Method for Moisture in the Analysis Sample of Coal and Coke*; ASTM International: West Conshohocken, PA, USA, 2017. Available online: [www.astm.org](http://www.astm.org) (accessed on 5 February 2020).
38. ASTM D3174-12(2018), *Standard Test Method for Ash in the Analysis Sample of Coal and Coke from Coal*; ASTM International: West Conshohocken, PA, USA, 2018. Available online: [www.astm.org](http://www.astm.org) (accessed on 5 February 2020).
39. ASTM D3175-18, *Standard Test Method for Volatile Matter in the Analysis Sample of Coal and Coke*; ASTM International: West Conshohocken, PA, USA, 2018. Available online: [www.astm.org](http://www.astm.org) (accessed on 5 February 2020).
40. Chung, F. Quantitative interpretation of X-ray diffraction patterns of mixtures: I. Matrix flushing method for quantitative multicomponent analysis. *J. Appl. Crystallogr.* **1974**, *7*, 519–525. [[CrossRef](#)]
41. Querol, X.; Whateley, M.K.G.; Fernandez-Turiel, J.L.; Tuncali, E. Geological controls on the mineralogy and geochemistry of the Beypazari lignite, Central Anatolia, Turkey. *Int. J. Coal Geol.* **1997**, *33*, 255–271. [[CrossRef](#)]
42. Chou, C.L. Sulfur in coals: A review of geochemistry and origins. *Int. J. Coal Geol.* **2012**, *100*, 1–13. [[CrossRef](#)]
43. Ward, C.R.; Christie, P.J. Clays and other minerals in coal seams of the Moura-Baralaba area, Bowen Basin, Australia. *Int. J. Coal Geol.* **1994**, *25*, 287–309. [[CrossRef](#)]
44. Dai, S.; Chou, C.L. Occurrence and origin of minerals in a chamosite-bearing coal of Late Permian age, Zhaotong, Yunnan, China. *Am. Miner.* **2007**, *92*, 1253–1261. [[CrossRef](#)]
45. Dai, S.; Li, T.; Seredin, V.V.; Ward, C.R.; Hower, J.C.; Zhou, Y.; Zhang, M.; Song, X.; Song, W.; Zhao, C. Origin of minerals and elements in the Late Permian coals, tonsteins, and host rocks of the Xinde Mine, Xuanwei, eastern Yunnan, China. *Int. J. Coal Geol.* **2014**, *121*, 53–78. [[CrossRef](#)]
46. Ward, C.R. Analysis, origin and significance of mineral matter in coal: An updated review. *Int. J. Coal Geol.* **2016**, *165*, 1–27. [[CrossRef](#)]
47. Liang, S.; Liu, Q.; Yu, C.; Song, H. Ammonium-bearing illite in tonsteins of Permo- Carboniferous coal accumulation area of Northern China. *J. Hebei Inst. Archit. Sci. Technol.* **2005**, *22*, 59–65. (In Chinese)
48. Dai, S.; Liu, J.; Ward, C.R.; Hower, J.C.; French, D.; Jia, S.; Hood, M.M.; Garrison, T.M. Mineralogical and geochemical compositions of Late Permian coals and host rocks from the Guxu Coalfield, Sichuan Province, China, with emphasis on enrichment of rare metals. *Int. J. Coal Geol.* **2016**, *166*, 71–95. [[CrossRef](#)]
49. Permana, A.K.; Ward, C.R.; Li, Z.; Gurba, L.W. Distribution and origin of minerals in high-rank coals of the South Walker Creek area, Bowen Basin, Australia. *Int. J. Coal Geol.* **2013**, *116*, 185–207. [[CrossRef](#)]
50. Liu, J.; Song, H.; Dai, S.; Nechaev, V.P.; Graham, I.T.; French, D.; Nechaeva, E.V. Mineralization of REE-Y-Nb-Ta-Zr-Hf in Wuchiapingian coals from the Liupanshui Coalfield, Guizhou, southwestern China: Geochemical evidence for terrigenous input. *Ore Geol. Rev.* **2019**, *115*, 103190. [[CrossRef](#)]
51. Li, B.; Zhuang, X.; Querol, X.; Moreno, N.; Yang, L.; Shangguan, Y.; Li, J. Mineralogy and Geochemistry of Late Permian Coals within the Tongzi Coalfield in Guizhou Province, Southwest China. *Minerals* **2019**, *9*, 44. [[CrossRef](#)]
52. Wang, X.; Dai, S.; Ren, D.; Yang, J. Mineralogy and geochemistry of Al-hydroxide/oxyhydroxide mineral-bearing coals of Late Paleozoic age from the Weibei coalfield, southeastern Ordos Basin, North China. *Int. J. Coal Geol.* **2011**, *26*, 1086–1096. [[CrossRef](#)]
53. Dai, S.; Zou, J.; Jiang, Y.; Ward, C.R.; Wang, X.; Li, T.; Xue, W.; Liu, S.; Tian, H.; Sun, X.; et al. Mineralogical and geochemical compositions of the Pennsylvanian coal in the Adaohai Mine, Daqingshan Coalfield, Inner Mongolia, China: Modes of occurrence and origin of diaspore, gorceixite, and ammonianillite. *Int. J. Coal Geol.* **2012**, *94*, 250–270. [[CrossRef](#)]
54. Kostava, I.; Petrov, O.; Kortenski, J. Mineralogy, geochemistry and pyrite content of Bulgarian subbituminous coals, Pernik Basin. In *Coalbed Methane and Coal Geology*; Gayer, R., Harris, I., Eds.; Geological Society Publication: London, UK, 1996; Volume 109, pp. 301–314.

55. Dai, S.; Wang, X.; Seredin, V.V.; Hower, J.C.; Ward, C.R.; O'Keefe, J.M.K.; Huang, W.; Li, T.; Li, X.; Liu, H.; et al. Petrology, mineralogy, and geochemistry of the Ge-rich coal from the Wulantuga Ge ore deposit, Inner Mongolia, China: New data and genetic implications. *Int. J. Coal Geol.* **2012**, *90–91*, 72–99. [[CrossRef](#)]
56. Spiro, B.F.; Liu, J.; Dai, S.; Zeng, R.; Large, D.; French, D. Marine derived  $^{87}\text{Sr}/^{86}\text{Sr}$  in coal, a new key to geochronology and palaeoenvironment: Elucidation of the India-Eurasia and China-Indochina collisions in Yunnan, China. *Int. J. Coal Geol.* **2019**, *215*, 103304. [[CrossRef](#)]
57. Seredin, V.V.; Dai, S. Coal deposits as potential alternative sources for lanthanides and yttrium. *Int. J. Coal Geol.* **2012**, *94*, 67–93. [[CrossRef](#)]
58. Taylor, S.R.; McLennan, S.M. *The Continental Crust: Its Composition and Evolution*; Blackwell: Oxford, UK, 1985; 312p.
59. Dai, S.; Hower, J.C.; Finkelman, R.B.; Graham, I.T.; French, D.; Ward, C.R.; Eskenazy, G.; Wei, Q.; Zhao, L. Organic associations of non-mineral elements in coal: A review. *Int. J. Coal Geol.* **2020**, *218*, 103347. [[CrossRef](#)]
60. Eskenazy, G.; Finkelman, R.B.; Chattarjee, S. Some considerations concerning the use of correlation coefficients and cluster analysis in interpreting coal geochemistry data. *Int. J. Coal Geol.* **2010**, *83*, 491–493. [[CrossRef](#)]
61. Kortenski, J.; Sotirov, A. Trace and major element content and distribution in Neogene lignite from the Sofia Basin, Bulgaria. *Int. J. Coal Geol.* **2002**, *52*, 63–82. [[CrossRef](#)]
62. Bauluz, B.; Mayayo, M.J.; Fernandez-Nieto, C.; Lopez, J.M.G. Geochemistry of Precambrian and Paleozoic siliciclastic rocks from the Iberian Range NE Spain: Implications for source-area weathering, sorting, provenance, and tectonic setting. *Chem. Geol.* **2000**, *168*, 135–150. [[CrossRef](#)]
63. Cullers, R. The geochemistry of shales, siltstones and sandstones of Pennsylvanian–Permian age, Colorado, USA: Implications for provenance and metamorphic studies. *Lithos* **2000**, *51*, 181–203. [[CrossRef](#)]
64. Cullers, R. Implications of elemental concentrations for provenance, redox conditions, and metamorphic studies of shales and limestones near Pueblo, CO, USA. *Chem. Geol.* **2002**, *191*, 305–327. [[CrossRef](#)]
65. Hayashi, K.; Fujisawa, H.; Holland, H.D.; Ohmoto, H. Geochemistry of ~1.9 Ga sedimentary rocks from northeastern Labrador, Canada. *Geochim. Cosmochim. Acta* **1997**, *61*, 4115–4137. [[CrossRef](#)]
66. McLennan, S.M.; Hemming, S.; McDaniel, D.K.; Hanson, G.N. Geochemical approaches to sedimentation, provenance and tectonics. *Geol. Soc. Am. Spec. Pap.* **1993**, *284*, 21–40.
67. Dai, S.; Ren, D.; Li, S. Discovery of the super large gallium ore deposit in Jungar, Inner Mongolia, North China. *Chin. Sci. Bull* **2006**, *51*, 2243–2252. [[CrossRef](#)]
68. Yan, X.; Dai, S.; Graham, I.T.; He, X.; Shan, K.; Liu, X. Determination of Eu concentrations in coal, fly ash and sedimentary rocks using a cation exchange resin and inductively coupled plasma mass spectrometry (ICP-MS). *Int. J. Coal Geol.* **2018**, *191*, 152–156. [[CrossRef](#)]
69. Cullers, R. The controls on the major and trace element variation of shale, siltstones, and sandstones of Pennsylvanian-Permian age from uplifted continental blocks in Colorado to platform sediment in Kansas, USA. *Geochim. Cosmochim. Acta* **1994**, *58*, 4955–4972. [[CrossRef](#)]
70. Middelburg, J.J.; van der Weijden, C.H.; Woittiez, J.R. Chemical processes affecting the mobility of major, minor and trace elements during weathering of granitic rocks. *Chem. Geol.* **1988**, *68*, 253–273. [[CrossRef](#)]
71. Nesbitt, H.W.; Wilson, R.E. Recent chemical weathering of basalts. *Am. J. Sci.* **1992**, *292*, 740–777. [[CrossRef](#)]
72. Dai, S.; Luo, Y.; Seredin, V.V.; Ward, C.R.; Hower, J.C.; Zhao, L.; Liu, S.; Zhao, C.; Tian, H.; Zou, J. Revisiting the late permian coal from the Huayingshan, Sichuan, southwestern China: Enrichment and occurrence modes of minerals and trace elements. *Int. J. Coal Geol.* **2014**, *122*, 110–128. [[CrossRef](#)]
73. Belousova, E.A.; Griffin, W.L.; O'Reilly, S.Y.; Fisher, N.I. Igneous zircon trace element composition as an indicator of source rock type. *Contrib. Mineral. Petrol.* **2002**, *143*, 602–622. [[CrossRef](#)]
74. Boyd, R.J. The partitioning behaviour of boron from tourmaline during ashing of coal. *Int. J. Coal Geol.* **2002**, *53*, 43–54. [[CrossRef](#)]
75. Finkelman, R.B. Modes of occurrence of trace elements in coal. In *US Geological Survey, Open File Report*; U.S. Geological Survey: Reston, VA, USA, 1981; pp. 81–99.
76. Finkelman, R.B. Mode of occurrence of potentially hazardous elements in coal: Levels of confidence. *Fuel Process. Technol.* **1994**, *39*, 21–34. [[CrossRef](#)]
77. Rügner, O. Tonmineral-Neubildung und Paläosalinität im Unteren Muschelkalk des Südlichen Germanischen Beckens. Ph.D. Thesis, University of Heidelberg, Heidelberg, Germany, 2000; 189p.

78. Shao, L.; Jones, T.; Gayer, R.; Dai, S.; Li, S.; Jiang, Y.; Zhang, P. Petrology and geochemistry of the high-sulphur coals from the Upper Permian carbonate coal measures in the Heshan Coalfield, southern China. *Int. J. Coal Geol.* **2003**, *55*, 1–26. [[CrossRef](#)]
79. Zeng, R.; Zhuang, X.; Koukouzas, N.; Xu, W. Characterization of trace elements in sulphur-rich Late Permian coals in the Heshan coal field, Guangxi, South China. *Int. J. Coal Geol.* **2005**, *61*, 87–95. [[CrossRef](#)]
80. Bouska, V.; Pesek, J. Boron in the aleuropelites of the Bohemian massif. In Proceedings of the 5th Meeting of the European Clay Groups, Prague, Czech Republic, 31 August–3 September 1983; pp. 147–155.
81. Goodarzi, F.; Swaine, D.J. The influence of geological factors on the concentration of boron in Australian and Canadian coals. *Chem. Geol.* **1994**, *118*, 301–318. [[CrossRef](#)]
82. Lyons, P.C.; Palmer, C.A.; Bostick, N.H.; Fletcher, J.D.; Dulong, F.T.; Brown, F.W.; Brown, Z.A.; Krasnow, M.R.; Romankiw, L.A. Chemistry and origin of minor and trace elements in vitrinite concentrates from a rank series from the eastern United States, England, and Australia. *Int. J. Coal Geol.* **1989**, *13*, 481–527. [[CrossRef](#)]
83. Eskenazy, G.M.; Delibaltova, D.; Mincheva, E. Geochemistry of boron in Bulgarian coals. *Int. J. Coal Geol.* **1994**, *25*, 93–110. [[CrossRef](#)]
84. Dai, S.; Liu, J.; Ward, C.R.; Hower, J.C.; Xie, P.; Jiang, Y.; Hood, M.M.; O’Keefe, J.M.K.; Song, H. Petrological, geochemical, and mineralogical compositions of the low-Ge coals from the Shengli Coalfield, China: A comparative study with Ge-rich coals and a formation model for coal-hosted Ge ore deposit. *Ore Geol. Rev.* **2015**, *71*, 318–349. [[CrossRef](#)]
85. Dai, S.; Guo, W.; Nechaev, V.P.; French, D.; Ward, C.R.; Spiro, B.F.; Finkelman, R.B. Modes of occurrence and origin of mineral matter in the Palaeogene coal (No. 19-2) from the Hunchun Coalfield, Jilin Province, China. *Int. J. Coal Geol.* **2018**, *189*, 94–110. [[CrossRef](#)]
86. Guo, W.; Dai, S.; Nechaev, V.P.; Nechaeva, E.V.; Wei, G.; Finkelman, R.B.; Spiro, B.F. Geochemistry of Palaeogene coals from the Fuqiang Mine, Hunchun Coalfield, northeastern China: Composition, provenance, and relation to the adjacent polymetallic deposits. *J. Geochem. Explor.* **2019**, *196*, 192–207. [[CrossRef](#)]
87. Dai, S.; Bechtel, A.; Eble, C.F.; Flores, R.M.; French, D.; Graham, I.T.; Hood, M.M.; Hower, J.C.; Korasidis, V.A.; Moore, T.A.; et al. Recognition of peat depositional environments in coal: A review. *Int. J. Coal Geol.* **2020**, *219*, 103383. [[CrossRef](#)]
88. Liu, H.; Zhang, Y.; Wang, H.; Jia, Y.; Long, Y. *Study of Lithofacies Paleogeography of Coal-bearing Formations of Jungar Coalfield*; Geological Publishing House: Beijing, China, 1991; 128p.
89. Wang, D.; Shao, L.; Li, X.; Li, Z. Palaeogeographic characteristics of the Middle Jurassic Yan’an Age in northern Shaanxi Province. *J. Palaeogeogr.* **2012**, *14*, 451–460.
90. Wang, X.; Tang, Y.; Jiang, Y.; Xie, P.; Zhang, S.; Chen, Z. Mineralogy and geochemistry of an organic- and V-Cr-Mo-U-rich siliceous rock of Late Permian age, western Hubei Province, China. *Int. J. Coal Geol.* **2017**, *172*, 19–30. [[CrossRef](#)]
91. Meng, Q.T.; Liu, Z.J.; Bruch, A.A.; Liu, R.; Hu, F. Palaeoclimatic evolution during Eocene and its influence on oil shale mineralisation, Fushun basin, China. *J. Asian Earth Sci.* **2012**, *45*, 95–105. [[CrossRef](#)]
92. Dai, S.; Hower, J.C.; Ward, C.R.; Gou, W.; Song, H.; O’Keefe, J.M.K.; Xie, P.; Hood, M.M.; Yan, X. Elements and phosphorus minerals in the middle Jurassic inertinite-rich coals of the Muli Coalfield on the Tibetan Plateau. *Int. J. Coal Geol.* **2015**, *144–145*, 23–47. [[CrossRef](#)]
93. Dai, S.; Ward, C.R.; Graham, I.T.; French, D.; Hower, J.C.; Zhao, L.; Wang, X. Altered volcanic ashes in coal and coal-bearing sequences: A review of their nature and significance. *Earth-Sci. Rev.* **2017**, *175*, 44. [[CrossRef](#)]
94. Finkelman, R.B.; Dai, S.; French, D. The importance of minerals in coal as the hosts of chemical elements: A review. *Int. J. Coal Geol.* **2019**, *212*, 103251. [[CrossRef](#)]

